JGR Oceans

RESEARCH ARTICLE
10.1029/2024JC021116

Modeling Planktonic Food Web Interannual Variability of the Northern Gulf of Alaska Shelf

Ludivine Conte[1], Jerome Fiechter[1], Suzanne Strom[2], Russell R. Hopcroft[3], Seth L. Danielson[3], and Ana Aguilar-Islas[3]

[1]Department of Ocean Sciences, University of California, Santa Cruz, Santa Cruz, CA, USA, [2]Shannon Point Marine Center, Western Washington University, Anacortes, WA, USA, [3]College of Fisheries and Ocean Sciences, University of Alaska Fairbanks, Fairbanks, AK, USA

Abstract A 25-year (1996–2020) hindcast from a coupled physical-biogeochemical model is evaluated with nutrients, phytoplankton and zooplankton field data and is analyzed to identify mechanisms controlling seasonal and interannual variability of the northern Gulf of Alaska (NGA) planktonic food web. Characterized by a mosaic of processes, the NGA is a biologically complex and productive marine ecosystem. Empirical Orthogonal Function (EOF) analysis combining abiotic and biotic variables averaged over the continental shelf reveals that light intensity is a main driver for nanophytoplankton variability during spring, and that nitrate availability is a main driver for diatoms during spring and for both phytoplankton during summer. Zooplankton variability is a combination of carry-over effects from the previous year and bottom-up controls from the current year, with copepods and euphausiids responding to diatoms and microzooplankton responding to nanophytoplankton. The results also demonstrate the effect of nitrate availability and phytoplankton community structure on changes in biomass and energy transfers across the planktonic food web over the entire growing season. In particular, the biomass of large copepods and euphausiids increases more significantly during years of higher relative diatom abundance, as opposed to years with higher nitrate availability. Large microzooplankton was identified as the planktonic group most sensitive to perturbations, presumably due to its central position in the food web. By quantifying the combined variability of several key planktonic functional groups over a 25-year period, this work lays the foundation for an improved understanding of the long-term impacts of climate change on the NGA shelf.

Plain Language Summary The northern Gulf of Alaska planktonic food web supports a highly productive and diverse marine ecosystem. Here we used a 25-year model simulation (1996–2020) to explore how its structure and variability (from phytoplankton to krill) are affected by the highly variable environmental conditions experienced over the continental shelf each season and across years. A statistical analysis identifies light intensity as a main driver for small phytoplankton variability during spring, and nutrient availability as a main driver for large phytoplankton (diatoms) during spring and for both phytoplankton types during summer. Changes in zooplankton are influenced by abundances from the previous year and prey availability from the current year. In general, larger zooplankton species (copepods and krill) respond to large phytoplankton availability and smaller zooplankton species respond to small phytoplankton availability. Finally, the biomass of large zooplankton increases more significantly during years when large phytoplankton is relatively more abundant, as opposed to years when more nutrients are available. By advancing knowledge about the seasonal and year-to-year response of several key planktonic functional groups over the recent historical period (1996–2020), this work lays the foundation for an improved understanding of the long-term impacts of climate change in the northern Gulf of Alaska region.

Key Points:

- Drivers of recent seasonal and interannual variability of the Gulf of Alaska planktonic food web are explored with a 25-year hindcast
- Light and nutrient availability are the main drivers of phytoplankton production, but their effect varies by season and functional group
- Trophic energy transfer to larger zooplankton is more sensitive to changes in phytoplankton composition than to changes in abundance alone

Supporting Information:

Supporting Information may be found in the online version of this article.

Correspondence to:

L. Conte,
ludivine.conte.2204@gmail.com

Citation:

Conte, L., Fiechter, J., Strom, S., Hopcroft, R. R., Danielson, S. L., & Aguilar-Islas, A. (2024). Modeling planktonic food web interannual variability of the northern Gulf of Alaska shelf. *Journal of Geophysical Research: Oceans*, *129*, e2024JC021116. https://doi.org/10.1029/2024JC021116

Received 22 MAR 2024
Accepted 22 JUL 2024

Author Contributions:

Conceptualization: Ludivine Conte, Jerome Fiechter
Data curation: Ludivine Conte, Jerome Fiechter
Formal analysis: Ludivine Conte, Jerome Fiechter
Funding acquisition: Jerome Fiechter, Suzanne Strom, Russell R. Hopcroft, Seth L. Danielson, Ana Aguilar-Islas
Investigation: Ludivine Conte, Jerome Fiechter
Methodology: Ludivine Conte, Jerome Fiechter, Suzanne Strom, Russell R. Hopcroft, Seth L. Danielson, Ana Aguilar-Islas

1. Introduction

Planktonic communities of the northwestern Gulf of Alaska (NGA; from ca. 142° to 162°W) support a highly productive and diverse ecosystem with vast numbers of fish, sea birds, and marine mammals. Because of these valued marine resources, the region has been the focus of extensive long-term monitoring programs such as the Global Ocean Ecosystem Dynamics (GLOBEC, from 1998 to 2004) and the Long-Term Ecological Research (LTER, started in 2017) programs making it an ideal study site to investigate the impact of climate variability and climate change on the structure and dynamic of the ecosystem and fishery production. However, it is challenging to understand the impacts of climate change on lower trophic levels and detect trends in responses when

Supervision: Jerome Fiechter
Validation: Ludivine Conte
Visualization: Ludivine Conte
Writing – original draft: Ludivine Conte
Writing – review & editing: Ludivine Conte, Jerome Fiechter, Suzanne Strom, Russell R. Hopcroft, Seth L. Danielson, Ana Aguilar-Islas

communities experience strong climate-driven natural variability in environmental conditions over a wide periodicity range, such as single-year ENSO events, multiyear marine heatwaves, and decadal-scale regime shifts (Batten et al., 2018; Di Lorenzo et al., 2008; Ducklow et al., 2022; Mantua et al., 1997). This is particularly the case over the continental shelf where a complex interplay of physical and biogeochemical processes controls nutrient availability in a system dominated by downwelling favorable winds (Fiechter et al., 2009; Stabeno et al., 2004; Weingartner et al., 2005). Due to the scarcity of concurrent environmental and ecosystem observations in the NGA region, coupled physical-biogeochemical models afford the ability to examine these processes and relationships in a comprehensive framework. Here, a 25-year hindcast (1996–2020) is used to elucidate how planktonic food web structure and variability are modulated by environmental conditions on seasonal to interannual time scales.

Natural variability in environmental conditions is primarily expressed at the seasonal time scale. In spring, increased photosynthetically available radiation due to shoaling mixed layer and decreasing cloud cover triggers a phytoplankton bloom (Henson, 2007). This bloom is dominated by diatoms in nearshore waters due to relatively high dissolved iron concentrations (Aguilar-Islas et al., 2016; Lippiatt et al., 2010), while iron limitation over the basin gives a competitive advantage to smaller phytoplankton cells (Hudson & Morel, 1993). Iron can be supplied to the shelf by sediment resuspension (Crusius et al., 2017) benthic flux (Aguilar-Islas et al., 2016), river input of glacial and snowfield melt during late summer and fall (Wu et al., 2009), and dust inputs during fall (Crusius et al., 2011). Nitrate concentrations over the shelf can be low enough to limit phytoplankton growth in late spring and summer (Childers et al., 2005; Waite & Mueter, 2013). Replenishment of macronutrients to the euphotic zone occurs in fall, winter and early spring when storms promote deep vertical mixing, and strong downwelling advect macronutrient-rich and iron-poor surface waters on-shelf from the center of the subpolar Alaska gyre (Auad, 2008; Stabeno et al., 2016; Wu et al., 2009). Other time-varying processes locally supply the surface shelf waters with macronutrient-rich oceanic waters. Cross-shelf exchange can result from episodic mesoscale eddies that propagate westward along the shelf (Fiechter et al., 2009; Okkonen et al., 2003), from the interaction of gullies and banks with the two major current systems (Cheng et al., 2012): the Alaska Coastal Current (ACC), flowing southwestward along the coast and forced by winds and freshwater inputs (Mordy et al., 2019) and the Alaskan Stream (AS), the western boundary current of the subpolar gyre flowing along the shelfbreak (Ladd et al., 2005; Reed, 1984), and from River plumes that can provide nutrients to the inner shelf (Brown et al., 2010). Zooplankton communities also exhibit strong seasonal variability (Coyle & Pinchuk, 2003; Strom et al., 2019). Microzooplankton (e.g., ciliates and dinoflagellates) are the main consumers of phytoplankton in the ocean (Schmoker et al., 2013) and their biomasses has been shown to increase along with phytoplankton biomasses during the spring NGA bloom (Strom et al., 2019). Experiments conducted along the Seward Line have notably shown that these grazers consumed nearly all production by small phytoplankton and about half of the diatom production (Strom et al., 2007). Mesozooplankton is mainly comprised of calanoid copepods although with significant contributions from other taxa such as cnidarians, euphausiids, pteropods and larvaceans (Coyle & Pinchuk, 2003, 2005; Doubleday & Hopcroft, 2015; Pinchuk et al., 2008). Changes in the mesozooplankton community composition and abundance are a result of complex abiotic and biotic factors and their timing (Sousa et al., 2016). While growth rates are strongly affected by temperature and food availability (e.g., Clarke & Peck, 1991; Hirst et al., 2003), they are also modulated by negative salinity anomalies associated with freshwater discharge (Coyle & Pinchuk, 2005; Kimmel & Duffy-Anderson, 2020) and by cross-shelf water transport (Cooney, 1986; Sousa et al., 2016).

Primary and secondary production in the NGA respond to inter-annual variations in the environmental drivers, such as cloud-mediated light intensity, temperature, eddy location and activity, and the intensity and timing of freshwater discharge and winds (e.g., Coyle et al., 2013; Kimmel & Duffy-Anderson, 2020; Strom et al., 2016; Waite and Mueter, 2013). For example, changes in wind magnitude and direction during winter and spring determine the amount of cross-shelf nutrient exchange and timing of stratification (Ladd et al., 2005; Stabeno et al., 2004; Weingartner et al., 2005). These variations are influenced by atmosphere–ocean climate feedbacks operating at scales that extend from the Gulf of Alaska (GOA) basin to the greater North Pacific Ocean. Climate variability on interannual to decadal time scales has been commonly tracked by indices derived from ocean condition statistics, such as the Pacific Decadal Oscillation (PDO) (Mantua et al., 1997) and the North Pacific Gyre Oscillation (NPGO) (Di Lorenzo et al., 2008). In the GOA, the PDO and NPGO positive phases are both associated with stronger coastal downwelling-favorable winds, intensified upwelling in the center of the subpolar gyre, and increased transport by its boundary currents (i.e., the Alaska Current in the eastern part and Alaskan

Stream in the western part, Stabeno et al., 2004). Furthermore, during positive PDO phases, an intense low-pressure system tends to be centered over the Alaska Peninsula, bringing warm, moist air to the coast with greater precipitation and stronger winds (Mantua et al., 1997). In the northeast Pacific, the PDO and NPGO have been related to changes in primary productivity (e.g., Aita et al., 2007; Di Lorenzo et al., 2008; Peña et al., 2019), community composition and abundances of zooplankton (e.g., Aita et al., 2007; Kimmel & Duffy-Anderson, 2020; Peterson & Schwing, 2003; Pinchuk et al., 2008) and commercially harvested species (e.g., Hare & Mantua, 2000; Kilduff et al., 2015; Litzow & Mueter, 2014; Mantua et al., 1997). A more recent study has established a new regional climate index focusing on the GOA: the Northern Gulf of Alaska Oscillation (NGAO), which relates changes in the intensity of the subpolar gyre circulation to large-scale atmospheric patterns that influence gyre upwelling variations over decadal time scales (Hauri et al., 2021). In a general sense, basin-scale variability modulates the fundamental processes that control seasonal ecosystem dynamics (e.g., onset of stratification, nutrient replenishment via winter downwelling, and summer river runoff) and, thus, the timing and amplitude of primary production during the spring bloom and subsequent development of zooplankton communities in the NGA (Coyle & Pinchuk, 2003). However, it is important to note that climate indices represent low-frequency and large-scale effects of atmospheric winds and oceanic circulation on ecosystem processes and may not effectively describe the important smaller-scale patterns and year-to-year differences in primary and secondary production in the coastal waters of the NGA (Coyle et al., 2013; Strom et al., 2016).

Ecosystem modeling is useful for exploring relationships between spatiotemporal changes in the physical and biogeochemical environments and lower trophic-level responses, and distinguishing long-term climate change effects from natural interannual variability. Several plankton dynamics models, coupled to 3-D representations of the ocean circulation, have been developed for the NGA ecosystem (Coyle et al., 2012, 2013, 2019; Fiechter and Moore, 2009, 2012; Fiechter et al., 2009; Hauri et al., 2020, 2021; Hinckley et al., 2009). Analyses of these simulations have identified key processes associated with planktonic food web response on seasonal and interannual time scales, such as pycnocline depth (Coyle et al., 2012, 2013), balance between iron input from freshwater runoff and nitrate concentrations (Coyle et al., 2012, 2019), wintertime wind stress curl and Ekman upwelling over the shelf (Fiechter & Moore, 2009), and shelfbreak eddy activity (Fiechter & Moore, 2012). However, aside from the more recent studies of Hauri et al. (2020, 2021) examining drivers of ocean acidification at regional and basin scales, most model analyses have focused on interannual variability across 5–15 years intervals, which are shorter than those needed to distinguish drivers of long-term natural climate variability and potential long-term effect of climate change. The present work builds upon and augments earlier modeling studies by using a 25-year integration (1996–2020) to explore processes controlling springtime and summertime lower trophic level variability, over a time interval known to contain significant interannual, decadal, and extreme event variability (e.g., 1997–1998 El Nino and 2014-2016 large marine heatwave). The model is used to quantify trophic energy transfers during typical conditions, years with anomalously low or high nitrate availability, and years with anomalously low or high diatom contributions to the total phytoplankton biomass. The model configuration and parameterization specific to the NGA region is presented in Section 2. An extensive evaluation of the simulation against available in situ observations is provided in Section 3, along with an analysis of the seasonal drivers of planktonic food web dynamics and a characterization of trophic structure energy and transfers under various environmental conditions. Key findings are discussed in Section 4 and concluding remarks are provided in Section 5.

2. Methods

2.1. Coupled Physical-Biogeochemical Model

The ocean circulation model is an implementation of the Regional Oceanic Modeling System (ROMS) (Haidvogel et al., 2000; Shchepetkin & McWilliams, 2005) and encompasses a region ranging from ca. 50 to 62°N and 140 to 164°W. ROMS is a hydrostatic, primitive equation model that uses a terrain-following vertical coordinate and a split-mode technique to efficiently solve for the baroclinic and barotropic components of the circulation. To resolve nearshore dynamics associated with freshwater inputs along the NGA coast, the ROMS configuration used here has a horizontal resolution of 4.5 km and 50 vertical terrain-following levels with clustering near the surface (Danielson et al., 2020).

The biogeochemical model, denoted NEMUGA, is based on the North Pacific Ecosystem Model for Understanding Regional Oceanography (NEMURO) (Kishi et al., 2007), but tailored to represent lower trophic food

web complexity and processes important to the NGA region. NEMUGA includes 3 limiting macro-nutrients (nitrate (NO_3), ammonium (NH_4), and silicic acid ($SiOH_4$)), 1 limiting micro-nutrient (iron), and 8 planktonic functional groups expressed in equivalent nitrogen concentrations: 2 phytoplankton size classes (nanophytoplankton and diatoms), 2 microzooplankton size classes (small and large), and 3 mesozooplankton size classes (small copepods, large copepods, and large diapausing copepods), and euphausiids (krill). NEMUGA also contains 2 particulate matter pools (particulate organic nitrogen (PON) and particulate silica (opal)) and a dissolved organic nitrogen (DON) pool. Uptake of nitrogen and silicate by phytoplankton is represented via a Michaelis–Menten formulation and silicon uptake by diatoms is converted to nitrogen using the Si:N ratio, which involves an inverse linear relationship between diatom Si:N ratio and local dissolved iron concentrations (Fiechter & Moore, 2009). Sinking of PON and opal is proportional to their local vertical concentration gradient with a constant sinking speed of 40 m d^{-1}. Temperature dependence of phytoplankton and microzooplankton growth has been removed from previous versions of NEMURO. While studies of individual (usually temperate) phyto- and microzooplankton isolates show strong temperature dependence of growth rates (e.g., Eppley, 1972; Rose & Caron, 2007), field data from the NGA do not support this relationship on a community level. Summer temperatures average 7–10°C higher than spring, and the species assemblage changes seasonally (e.g., replacement of diatoms by small phytoflagellates) such that spring versus summer dominant species have roughly equal maximum growth rates (Strom et al., 2006 their Table 5; Strom et al., 2007 their Figure 7 (note that net growth rates of large microzooplankton size classes approximate intrinsic growth rates)).

NEMUGA is coupled to the ocean circulation by solving a transport equation in ROMS for all biogeochemical variables at every time step. The coupling is "one-way" in the sense that the physics impacts biological processes computed in NEMUGA but not the opposite. NEMUGA enhancements over previous versions of NEMURO implemented in the NGA (e.g., Fiechter et al., 2009) provide an improved regionally specific representation of some biogeochemical dynamics and lower trophic food web complexities. First, chlorophyll-a concentration is now calculated with a variable chlorophyll-to-carbon ratio (Chl:C) based on nutrient and light limitations, and light attenuation with depth instead of phytoplankton biomass (Jackson et al., 2017). Second, the iron limitation model (Fiechter et al., 2009) has been augmented with a leachable particulate iron pool to better represent inputs from rivers. Third, the micro- and meso-zooplankton functional groups were diversified to represent NGA planktonic food web complexity more accurately. These modifications are described in more detail in the following sections.

2.1.1. Chlorophyll-a Concentration and Light Attenuation

Chlorophyll-a concentration (Chl) associated with the two phytoplankton groups are diagnostically determined (Jackson et al., 2017), such that Chl:C (θ) is calculated as:

$$\theta = \frac{\theta_m}{I_*}\left(1 - e^{-I_*}\right) \tag{1}$$

where θ_m is the maximal Chl:C ratio (set to 0.025 and 0.05 g Chl g C^{-1} respectively for nanophytoplankton and diatoms) and I_* is a dimensionless scaled irradiance. I_* is computed as:

$$I_* = \frac{I \times \alpha}{P_m} \tag{2}$$

with α representing the initial slope of the photosynthesis-irradiance (P-I) curve (adjusted to 0.04 and 0.05 (W m^{-2})$^{-1}$ d^{-1}, respectively), for nanophytoplankton and diatoms, to improve the comparison with observed Chl). Since phytoplankton in the mixed layer experience a wide range of irradiance over times scales presumably too short (i.e., minutes to hours) to acclimate their Chl:C ratio, the calculation of θ in the mixed layer uses a vertically averaged light I (a typical acclimation time is of the order of 1 day (see refs. in Jackson et al., 2017). Below the mixed layer, I is simply PAR at the corresponding depth z. The phytoplankton growth rate, P_m, is computed as a function of nutrient and light limitation according to:

$$P_m = V_{\max} \cdot L_{\text{nut}} \cdot L_{\text{light}} \tag{3}$$

where V_{max} is the maximal growth rate (0.6 and 0.8 d^{-1} respectively for nanophytoplankton and diatoms). The carbon concentration is calculated from the phytoplankton-associated nitrate concentration using a constant C:N Redfield ratio of 6.6 mol C mol N^{-1}.

The total Chl concentration (i.e., nanophytoplankton plus diatom contributions) is subsequently used to attenuate light penetration in the water column due to biological activity based on the formulation of Morel and Maritorena (2001), with a coefficient of attenuation k computed from the coefficients for pure water K_w and biogenic compounds according to:

$$k(\theta) = K_w + \chi[\theta]^e \tag{4}$$

with the coefficients K_w, χ and e as published by Morel and Maritorena (2001) are known for wavelengths ranging between 350 and 800 nm.

2.1.2. Iron Limitation Model

The iron limitation model previously developed by Fiechter et al. (2009) for the NGA region includes two forms of iron: dissolved iron (F_D) and iron incorporated within phytoplankton cells (F_P). It also accounts for luxury uptake, which allows phytoplankton cells to absorb and store excess iron under nutrient-replete conditions. Therefore, iron limitation on phytoplankton growth is computed explicitly with separate budgets for nitrate and iron. The formulation (Fiechter et al., 2009) is improved here by adding a leachable particulate iron (F_L) component to more realistically account for inputs of both particulate and dissolved iron from rivers. The particulate leachable pool is not available for phytoplankton growth but can become available over short time scales (Hurst & Bruland, 2007) through mobilization to the dissolved phase by dissolution and remineralization processes (at a rate $d_r = 0.2$ d^{-1}). In turn, the dissolved pool, which is mainly composed of iron organically complexed with strong Fe-binding ligands (Aguilar-Islas et al., 2016), may be aggregated with dissolved organic matter, adsorb onto particles and be transferred to the leachable particulate pool (at a rate $a_g = 1.0$ d^{-1}). Conceptually:

$$\frac{\partial F_P}{\partial t} = F_P(U - G - M) + L_{Fe} \text{ for iron incorporated within phytoplankton cells,} \tag{5}$$

$$\frac{\partial F_L}{\partial t} = a_g F_D - d_r F_L + f_{\text{err}} G M F_P \text{ for the leachable iron pool and} \tag{6}$$

$$\frac{\partial F_D}{\partial t} = -U F_P - L_{Fe} + d_r F_L - a_g F_D \text{ for dissolved iron pool} \tag{7}$$

with U, G, M, and L_{Fe} respectively the nutrient limitation, grazing, mortality, and iron uptake terms described in Fiechter et al. (2009). A fraction of the phytoplankton-associated iron, f_{err}, returns to the dissolved phase as a result of mortality and grazing, with the remainder assumed to be instantly exported via sinking.

Strong winds events in winter and spring have been shown to produce elevated iron concentrations from sediment resuspension along the continental shelf (Crusius et al., 2017). To simulate this source of iron to surface waters, dissolved iron concentration (referred after as dFe) is restored year-round to 2 μmol Fe m^{-3} on a 5-day time scale in the bottom 20 m of the water column for shelf regions shallower that 200 m depth. While the choice of 200 m depth is somewhat arbitrary, it is meant to account for shelf regions over which near-bottom dFe concentrations could potentially be mixed into the euphotic zone and enhance primary production. The model does not include an iron source from dust deposition, although dust storms are known to deliver glacial flour with high Fe loadings to the NGA surface waters especially during fall when riverbank sediments are dried and exposed to winds while river water levels and snow cover are low (Crusius et al., 2011, 2017).

2.1.3. Zooplankton Diversity

Based on existing information from earlier studies in the NGA and on-going field studies from the NGA-LTER program, the formulation complexity of NEMUGA has been augmented over the original NEMURO configuration by adding zooplankton functional groups deemed necessary to better represent lower trophic level

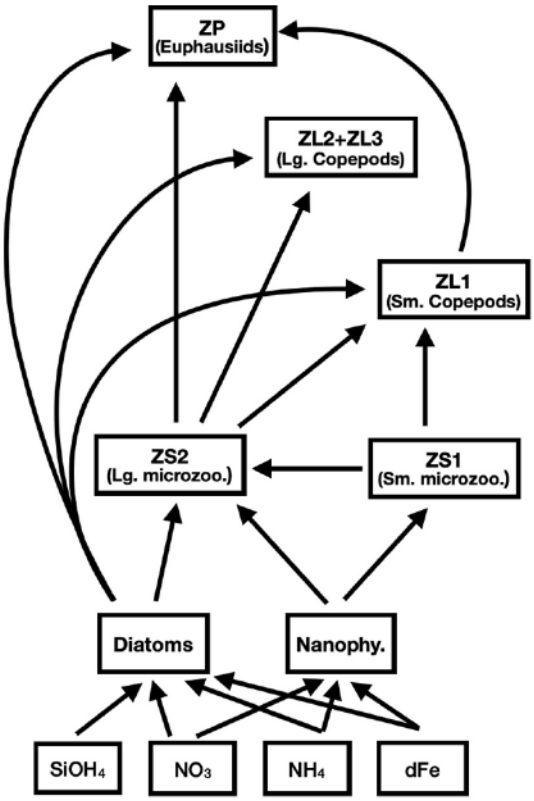

Figure 1. Schematic representation of the NEMUGA model formulation. Arrows indicate uptake and grazing fluxes associated with the various phytoplankton and zooplankton functional groups. The large zooplankton functional group is differentiated by the fact that ZL3 undergoes diapause and ZL2 does not.

community structure, variability, and resilience (Figure 1). Specifically, the original microzooplankton group (ZS) has been separated into a small microzooplankton group (ZS1, representing organisms <20 μm) and a large microzooplankton group (ZS2, representing organisms >20 μm). Microzooplankton (primarily protists) span over two orders of magnitude in maximum dimension (i.e., 2–200 μm) with corresponding trophic diversity. To a first approximation, protists at the lower end of this size spectrum (here ZS1, mainly heterotrophic nanoflagellates) can consume only bacteria and the smallest phytoplankton, and they are too small for efficient capture by larger crustacean zooplankton species in the NGA. In contrast, larger protists (here ZS2, mainly ciliates and dinoflagellates) can consume both small and large plankton (hetero- and autotrophic nanoflagellates, diatoms) and are readily—even preferentially—grazed by crustacean zooplankton (Hansen et al., 1994; Liu et al., 2005, 2008). Furthermore, the original mesozooplankton group (ZL) has been separated into a small copepod group (ZL1, representing *Pseudocalanus spp.*), a large copepod group (ZL2, representing *Calanus spp.*), and a large diapausing copepod group (ZL3, representing *Neocalanus spp.*), to account for differences in preferred prey and in life history. The ZL3 group enters the system early each spring, capitalizing on the emerging spring phytoplankton bloom for growth, then diapausing at depth by late spring. In contrast, ZL1 and ZL2 capitalize on the spring bloom for reproduction, and secondarily growth, extending their presence well into fall. ZL1 can eat smaller prey than ZL2.

Parameters controlling phytoplankton growth and zooplankton grazing were initially set based on expert knowledge. The updated model formulation thus affords, for example, the ability to examine trophic transfer of primary production to small copepods via smaller organisms (nanophytoplankton → small flagellates → small copepods) versus larger organisms (diatoms → ciliates/dinoflagellate → small copepods, or diatoms → small copepods directly). In the NGA, these two trophic pathways (small copepods feeding on small vs. large organisms) may increase small copepod resilience by providing a buffering mechanism against seasonal and interannual variability. Grazing depends on the relative abundance of the different prey that zooplankton feed on, thereby allowing for grazing to adjust according to simulated prey availability (Rose et al., 1999). Hence, grazing is proportional to the zooplankton biomass (Z), maximum grazing rate ($G_{\max}$, in units of d^{-1}), and a functional response between 0 and 1 that combines feeding factors for each prey i based on the prey biomass (P_i), its vulnerability (K_i, in units of P_i), and a non-dimensional feeding preference ($0 \le \upsilon_i \le 1$):

$$\text{Grazing} = G_{\max} \cdot Z \cdot \frac{\sum_i P_i.\upsilon_i/K_i}{1 + \sum_i P_i.\upsilon_i/K_i} \cdot e^{K_g T} \quad (8)$$

Daily grazing rates for copepods (ZL1, ZL2, ZL3) and euphausiids (ZP) are also temperature-dependent and follow a Q_{10} relationship (K_g of 0.0693 $degC^{-1}$). For microzooplankton (ZS1, ZS2), grazing is assumed to be independent of temperature ($K_g = 0$ $degC^{-1}$). All zooplankton groups convert total prey grazed into biomass with a constant growth efficiency of 0.3 (i.e., 30% of total prey biomass consumed is turned into predator biomass). Additional losses for zooplankton occur through a temperature-dependent (Q10 relationship) quadratic natural mortality term to account for density-dependent effects. Diapause of large copepods is represented by setting ZL3 biomass at 0 mmol N m^{-3} every year from July 9th (DOY 189). Every January 1st, ZL3 biomass are imposed equal to non-diapausing copepods ZL2 biomass. Hence, the current formulation does not attempt to model favorable or detrimental to ZL3 during overwintering and diapause emergence. The main purpose of including ZL3 diapause is to alleviate grazing pressure from ZL3 on diatoms and large microzooplankton (ZS2) in late summer and fall. For the present study, the biomasses of ZL2 and ZL3 have been summed for simplicity and the

total biomass of large copepods is referred hereafter as "ZL2_3". Values of the parameters for the ecosystem model are presented in Supporting Information S1.

2.2. Hindcast

The hindcast consists of monthly means extracted from a 27-year simulation (1994–2020). The first two years (1994 and 1995) were excluded from analysis to remove spin-up effects and to allow establishment of the physical and biological seasonal cycles. ROMS is driven on all open boundaries by 7-day averaged sea-surface height, velocity, temperature, and salinity fields from the GLORYS global ocean physics reanalysis (European Union-Copernicus Marine Service, 2018b, https://doi.org/10.48670/moi-00021). Although the GLORYS reanalysis only starts in 1993, it has the advantages of extending close to the present (2020), being relatively high resolution (1/12°), and having physical fields constrained by data assimilation (presumably yielding a more accurate representation of the subpolar gyre circulation at the open boundaries). Initial conditions are imposed by mapping the GLORYS fields for 1 January 1994, onto the ROMS grid. Tidal forcing is imposed using the TPXO 7.2 tidal inversion from Oregon State University based on satellite altimeter sea surface height observations (Egbert & Erofeeva, 2002). Freshwater inputs at the coast are implemented as momentum, temperature and salinity point sources (Danielson et al., 2020) based on daily river discharge values from the hydrological model of Beamer et al. (2016). Surface forcings are derived from the ERA5 global reanalysis (Hersbach et al., 2020), which consists of 3-hourly winds, air temperature, sea level pressure, specific humidity, precipitation, and short-wave and downwelling long-wave radiation.

Initial and boundary conditions for nutrients (nitrate, silicic acid, and dissolved iron) are based on monthly averages from a global ocean biogeochemistry hindcast (European Union-Copernicus Marine Service, 2018a, https://doi.org/10.48670/moi-00019). Initial conditions for the phytoplankton functional groups are derived by locally partitioning total phytoplankton biomass from the global hindcast as a function of the nitrate and iron limitation imposed in NEMUGA. Since total zooplankton biomass is not available in the global hindcast, initial conditions for the zooplankton functional groups are estimated using phytoplankton biomass, prey preferences set in NEMUGA, and a trophic transfer efficiency of 20%. Phytoplankton and zooplankton biomasses at the open boundaries are imposed using a zero-gradient condition (i.e., boundary values are set to those calculated in the adjacent cell inside the domain) to minimize numerical instabilities and accommodate for the lack of specific information from the global reanalysis across the NEMUGA functional groups. The initial and boundary conditions for leachable particulate iron are based on observed dissolved iron concentrations, assuming particulate iron concentrations are 10 times higher than dissolved iron concentrations inshore of the 200 m isobath and equal to dissolved iron concentrations offshore of the 1000 m isobath, with a linear transition in between to approximate in situ observations (e.g., Aguilar-Islas et al., 2016). Nutrient concentrations supplied by freshwater inputs at the coast are set to 0 mmol N m^{-3} for nitrate, 35 mmol Si m^{-3} for silicic acid, and 100 and 10 μmol Fe m^{-3}, respectively, for leachable particulate and dissolved iron concentrations.

2.3. Model Evaluation

In situ data along the Seward line were obtained from GLOBEC (1998–2004, http://usglobec.org/gaag/glance.php) and NGA-LTER (2018–2020, https://nga.lternet.edu) cruises, and from additional cruises for the period 2005–2017. Since the Seward Line is more routinely and uniformly sampled across all biotic and abiotic variables, the model is primarily evaluated against observations from Seward Line shelf stations GAK1 to GAK7 (Figure 2). Macronutrient data ($SiOH_4$ and NO_3) are available for 1998–2004 and 2012–2020. Chl concentration, copepod and euphausiid biomass are available from 1998 to 2020. Microzooplankton was sampled from 2011 onward for dinoflagellates and ciliates in the size fraction >20 μm, which were used to evaluate simulated ZS2. From 2018, nanoflagellates were also sampled, which were used to evaluate simulated ZS1. Simulated ZS1 and ZS2 biomasses in units of mmol N m^{-3} were converted to biomasses in units of μg C L^{-1} using a C:N ratio of 6, which is a compromise between autotroph dinoflagellates (average C:N ~ 7.5, Carnicer et al., 2022) and heterotroph ciliates (C:N ~ 5, Verity & Lagdon, 1984). Metazoan zooplankton data is derived from two different time-series sampling the upper 100 m of the water column. ZL1 was extracted for calanoids collected during daytime by CalVet-Quad nets that employ 150 μm mesh, while ZL2, ZL3 and ZP were extracted from night-time MOCNESS/Multinets of 500 μm mesh (see Sousa et al., 2016). Species contributing to the three larger zooplankton categories were excluded from the ZL1 summation. Simulated ZL and ZP biomasses in units of

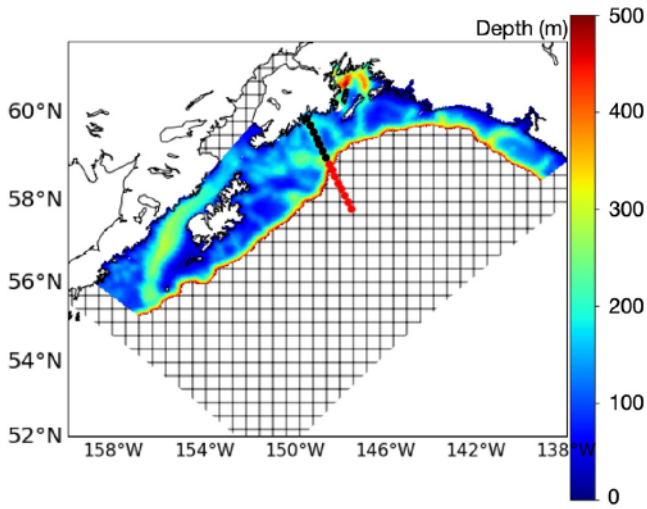

Figure 2. ROMS-NEMUGA model domain (black grid) and coastal subregion used for the analysis with bottom topography highlighted. Filled circles represent location of stations along the Seward Line (GAK1-GAK15). Black symbols denote shelf stations GAK1 to GAK7 used for model evaluation and red symbols denote stations GAK8-GAK15.

mmol N m^{-3} were converted to biomasses in grams wet weight m^{-3} by assuming that the dry weight is 20% of the wet weight and that the nitrogen dry weight is 7% of the total dry weight (Ito et al., 2010; Megrey et al., 2007).

The model fields are first evaluated in terms of their seasonal variability, at the surface (0–10 m) for Chl, macronutrients and microzooplankton and over the upper 100 m of the water column for copepods and euphausiids. After extracting the model cells corresponding to each GAK station, monthly climatologies were produced by averaging the 0–10 m (or 0–100 m) mean biomasses along GAK1-GAK7 stations over available years for each simulated and observed variable. The model output is also evaluated in terms of interannual variability, focusing on spring (April-May for nutrients, Chl and mesozooplankton and May only for microzooplankton) as it is the season for which in situ data are the most consistently available throughout the simulation period, at the surface (0–10 m) for macronutrients and microzooplankton, over the upper 50 m of the water column for Chl and over the upper 100 m of the water column for copepods and euphausiids.

For Chl, evaluation is completed with remotely sensed observations from MODIS Aqua (https://coastwatch.pfeg.noaa.gov/erddap/griddap/erdMH1Chl8day.graph) over 2003–2020, to assess the ability of the model to reproduce region-wide spatial and temporal patterns of variability. Simulated sea surface height (SSH) and sea surface temperature (SST) for 1996–2020 are evaluated against satellite observations available from Aviso (https://www.aviso.altimetry.fr/en/data/data-access.html) for SSH and from NOAA OISST (https://psl.noaa.gov/data/gridded/data.noaa.oisst.v2.html) for SST.

2.4. Interannual Variability Analysis

The analysis focuses on lower trophic level ecosystem variability for the period 1996–2020 associated with NGA shelf waters (defined here as the region between the coast and 500-m isobath), except for Cook Inlet for which the model solution is difficult to evaluate based on existing observations (Figure 2). Grid cells located within 100 km of the model boundaries were removed to prevent contamination from numerical edge effects.

Statistical Empirical Orthogonal Functions (EOFs) are used to investigate interannual co-variability across biotic and abiotic variables over the NGA shelf during spring and summer. While EOFs are traditionally used to identify the dominant modes of spatial and temporal variability for a particular variable (e.g., sea surface temperature or Chl), the analysis can also be applied to isolate primary modes of temporal variability common to a set of variables. Here, the EOF analysis (performed with Python "eofs" library) combines time series for temperature, mixed layer depth (MLD), photosynthetically available radiation (PAR), NO_3, $SiOH_4$, NH_4, dFe, and all planktonic functional groups to determine their leading modes of temporal co-variability during spring and summer, respectively. All modes representing more than 10% of the total variance were kept for the analysis. For nutrients concentrations and for phytoplankton and zooplankton biomasses, time series represent integrated values over the upper 50 m of the water column, averaged over the shelf domain (Figure 2) and summed over the months considered for each season: March to May for spring and July to September for summer (hereafter referred as "cumulated values"). 50 m was chosen as it represents the approximate depth at which chlorophyll concentrations in the water column have decreased by at least an order of magnitude relative to their maximum values (see Figure 3f). For temperature, the time series represents mean values over the upper 50 m of the water column, averaged spatially over the shelf domain and over the months considered for each season. For MLD and PAR, the time series represent values averaged spatially over the shelf domain and over the months considered for each season. MLD was calculated for each grid cell in the domain by considering the depth at which density exceeds the density at 10 m depth by 0.02 kg m^{-3}, with higher values representing a deeper MLD (i.e., MLD is treated as a positive number). PAR represents the short-wave radiation reaching the surface of the ocean. Each time series was also standardized by its temporal mean and standard deviation to render it unitless as a requirement for combining disparate variables in the EOF analysis. The temporal amplitude of each EOF mode was additionally regressed independently against each variable included in the analysis to identify the fraction of

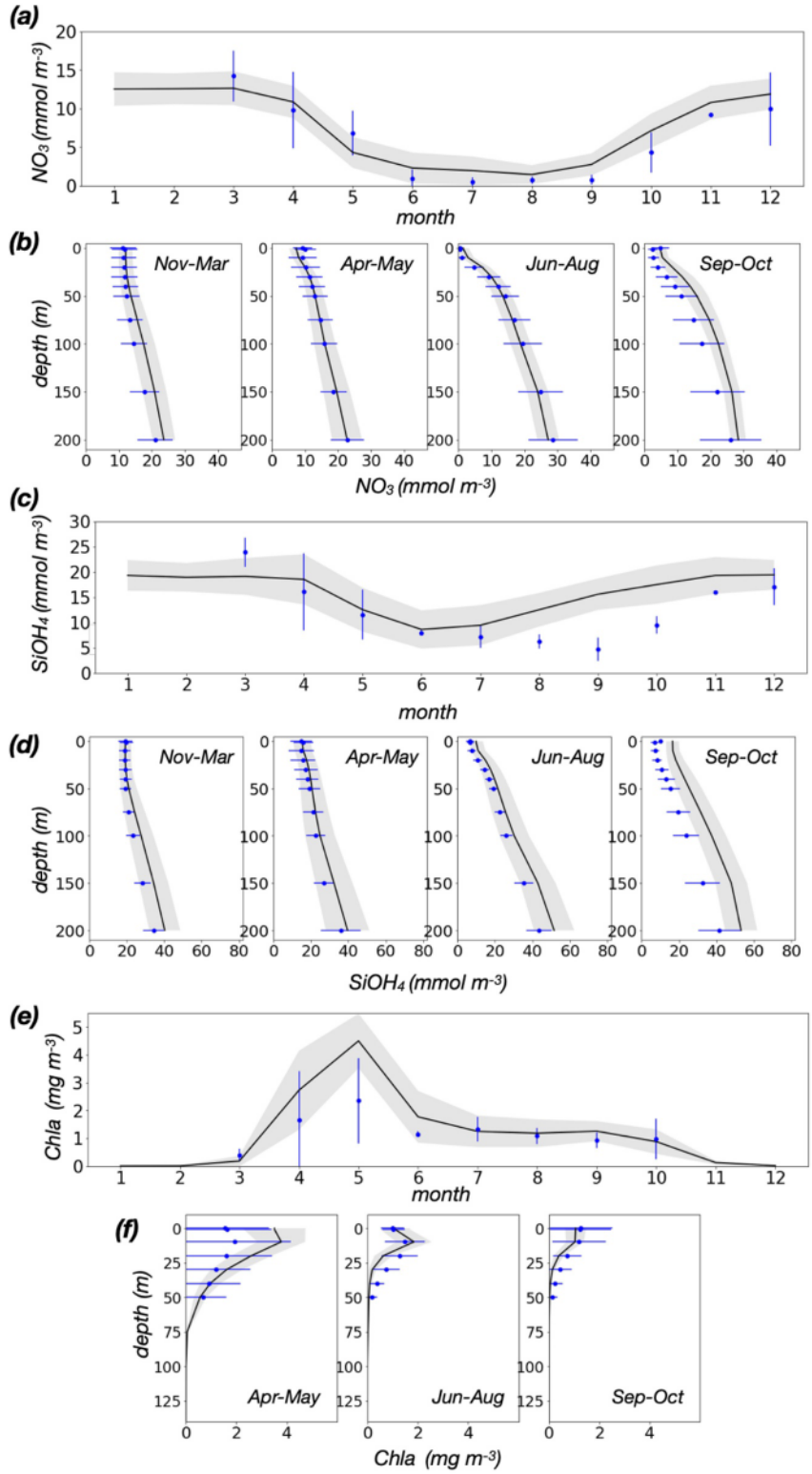

Figure 3. Simulated (black lines) and observed (blue symbols) nitrate (a, b), silicate (c, d), and Chl (e, f) concentrations averaged along GAK1 to GAK7 near the surface (0–10 m, a, c, and e) and with depth (b, d, and f). Standard deviations (in shaded gray for the model and blue lines for observations) represent the combined spatial and interannual variability. For nutrients, climatologies are based on 1998–2004 and 2012–2020 (n = 1,015 observations at the surface). For Chl, climatologies are based on 1998–2020 (n = 970 at the surface).

the total variance of that variable attributable to a particular EOF pattern. Time series used for the EOF analyses are presented in Figure S1 in Supporting Information S1.

Planktonic food web structure and trophic transfers are characterized using cumulated biomasses and grazing fluxes (i.e., integrated over the upper 50 m of the water column, averaged over the shelf domain, and summed over the months considered for spring, summer, and both seasons combined (March to September)). These biomasses and fluxes are first used to describe the mean planktonic food web for 1996–2020, and then to contrast years with anomalously low or high nitrate availability and years with anomalously low or high diatom abundance relative to total phytoplankton biomass. Anomalous years for nitrate concentrations and diatom fraction are selected based on whether their annual (March-September) mean values fall above or below their respective long-term means.

3. Results

3.1. Model Evaluation

This section presents comparisons of the monthly mean model outputs with *in-situ* data. Comparisons with satellite data are presented in Figure S2 in Supporting Information S1 (Chl) and Figure S3 in Supporting Information S1 (SSH and SST).

3.1.1. Seasonal Variability

Near the surface (0–10 m depth), the model reproduces the maximum nitrate and silicate concentrations (Figure 3) observed in winter, as well as the observed draw-down from April to June. From July to September, both observed and simulated nitrate reach their lowest concentration; however, the model overestimates the minimum observed values (by ∼1.2 mmol N m^{-3}). The largest discrepancy between model and observations occurs during late summer and early fall for silicate concentrations when in situ values continue to decrease until September while simulated values start increasing after July (mean simulated concentration for August-October is 15.2 mmol Si m^{-3} compared to 6.8 mmol Si m^{-3} for the observations). These model-data differences are primarily associated with stations GAK1-2 on the innermost shelf (not shown in figure). Simulated profiles indicate that the model reproduces the vertical structure and magnitude of observed nitrate and silicate concentrations with depth throughout the year (Figure 3), except during fall when simulated profiles have the correct vertical shape but are biased high compared to the observations.

For Chl, simulated values reproduce the observed seasonal cycle at the surface (0–10 m depth) (Figure 3), with a spring bloom initiated in April and a peak in May. However, the model overestimates the intensity of the spring bloom, with an averaged simulated concentration during April-May of 3.6 mg m^{-3} compared to 2.0 mg m^{-3} for the observation. The simulation adequately represents the period of lower and more stable observed concentrations from June through October, with averaged simulated and observed values of by ∼1.2 mg m^{-3}. Simulated profiles indicate that the model reproduces the overall vertical structure of observed Chl concentrations (including the weak but noticeable subsurface maximum near 10 m depth), but overestimates observed values near the surface (0–30 m depth) by ∼1.7 mg m^{-3} during spring and underestimate them at depth (below 20 m) by ∼0.3 mg m^{-3} during summer.

Nanoflagellate biomass is only available for the months of May and July. In May, simulated ZS1 biomass is in close agreement with the observed nanoflagellate biomass (Figure 4). In July, the model underpredicts the observed nanoflagellate biomass by a factor of about 3, although a large standard deviation is observed. Simulated ZS2 biomass peaks in June with a value of 21.3 μg C L^{-1} and decreases into summer and fall (Figure 4). Observed ciliate and dinoflagellate biomass (>20 μm) are available for April, May, July, and September. In April and May, the model exhibits very close agreement with observations. In July, it overestimates observed biomasses by a factor of about 4, although only a few in situ data points are available. In September, simulated ZS2 biomass substantially underestimates observed values by a factor of about 4, although a large standard deviation is observed.

For copepods and euphausiids, observations are more available and provide sufficient information to evaluate seasonality from March to October (Figure 4). The model generally reproduces the magnitude of observed copepod and euphausiid biomass but tends to underestimate their spatiotemporal variability (although in situ values can exhibit large standard deviations, such as for small copepods in July and large copepods in May). Simulated biomasses of ZL1 and ZP reproduce the observed seasonality of small copepods with a peak in July,

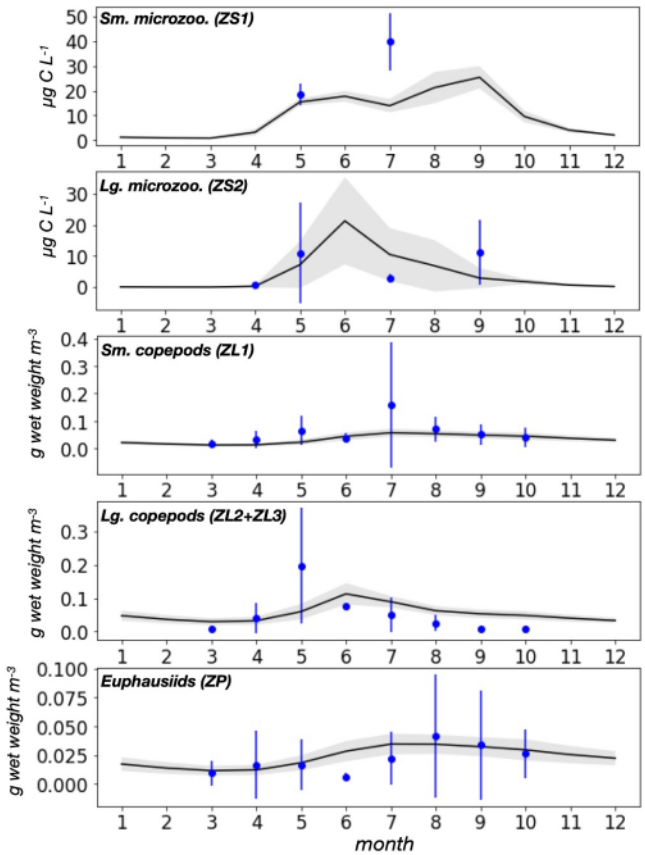

Figure 4. Simulated (black lines) and observed (blue symbols) small and large microzooplankton averaged along GAK1 to GAK7 near the surface (0–10 m) and small and large copepods and euphausiids biomasses along GAK1 to GAK7 averaged over 0–100 m. Standard deviations (in shaded gray for the model and blue lines for observations) represent the combined spatial and interannual variability. For small microzooplankton, climatologies are based on 2018–2020 ($n = 49$ observations), for large microzooplankton they are based on 2011–2020 ($n = 262$) and for all mesozooplankton they are based on 1998–2020 ($n = 477$ for small copepods; $n = 459$ for large copepods and euphausiids).

and of euphausiids with higher biomasses in summer and fall, respectively. The largest discrepancies between model and observations occur in May and July for ZL1 (although note the large range of in situ data for July), and June and July for ZP. Simulated biomass of ZL2 + ZL3 exhibits a maximum in June, a month later than the observations, and underestimates the magnitude of the peak (although observed values are quite variable). The model generally reproduces the observed rate of decrease of large copepods biomass through summer and fall but overestimates their magnitude by a factor of about 3.

3.1.2. Interannual Variability

Simulated nitrate and silicate concentrations exhibit similar interannual variability, with higher concentrations in 2007–2008 and in 2019 (Figure 5). The evaluation of interannual nutrient variability is limited because observations are only available for 1998–2004 and 2012–2020. The simulated mean values generally fall within one observed standard deviation from the in situ mean value (and vice versa). Simulated Chl concentrations generally agree with the dominant observed patterns, except for 2006, 2011, 2019 and 2020 where the model clearly overpredicts observations, and for 2002 and 2013 where observations are substantially above the average and outside the modeled standard deviation (Figure 5).

Nanoflagellate biomass exist only for 2019 and 2020, which prevents a meaningful evaluation of the simulated ZS1 biomass on an interannual basis (Figure 6). Simulated ZS2 and observed large ciliates and dinoflagellates biomasses exhibit strong interannual variability during spring. The model reproduces the higher large microzooplankton biomass observed in 2013 relative to 2011, and the much lower biomass observed during 2015–2020 relative to 2011 and 2013. Simulated ZL1 biomass generally agrees with the dominant observed patterns of small copepods during 1997–2020, except for a few individual years (e.g., 2000, 2009, 2016 and 2018). Simulated large copepods biomass (ZL2 + ZL3) during spring resembles that of ZL1 ($r = 0.95$, $p \leq 0.05$). While this behavior is less strong in the observations ($r = 0.43$, $p \leq 0.05$), the model is able to reproduce certain periods of lower (e.g., 2000–2004, 2012–2014) and higher (e.g., 2005–2006, 2017–2018) biomass, but clearly misrepresents other observations (e.g., lower observed biomass during 2007–2010 and higher observed biomass during 2015–2016). Simulated ZP biomass resembles that of small (ZL1) and large (ZL2 + ZL3) copepods ($r = 0.87$, $p \leq 0.05$ with ZL1 and $r = 0.92$, $p \leq 0.05$ with ZL2 + ZL3), but not in the observations ($r = -0.25$, $p = 0.27$ with small copepods and $r = -0.05$, $p = 0.82$ with large copepods). Considering the substantial observed variability along the Seward Line, the model provides qualitatively reasonable estimates of observed biomasses at GAK1-GAK7.

3.2. Interannual Springtime Variability

3.2.1. Mean Springtime Biomasses and Grazing Fluxes

The mean nanophytoplankton biomass during spring (Figure 7) is 26% lower than the diatom biomass. Nanophytoplankton is mainly consumed by ZS1 (with a flux 10 times as high as the flux from nanophytoplankton to ZS2). Diatoms are the main food source for ZS2 (consuming ~10 times as much diatoms as ZS1 and about 2 times as much diatoms as nanophytoplankton), ZL1 (consuming ~10 times as much diatoms as its other preys combined), ZL2_3 (consuming ~20 times as much diatoms as ZS2) and ZP (consuming ~25 times as much diatoms as its other preys combined). ZL1 consumes ZS1 and ZS2 in same amounts and ZP consumes ZS2 and ZL1 in same amounts.

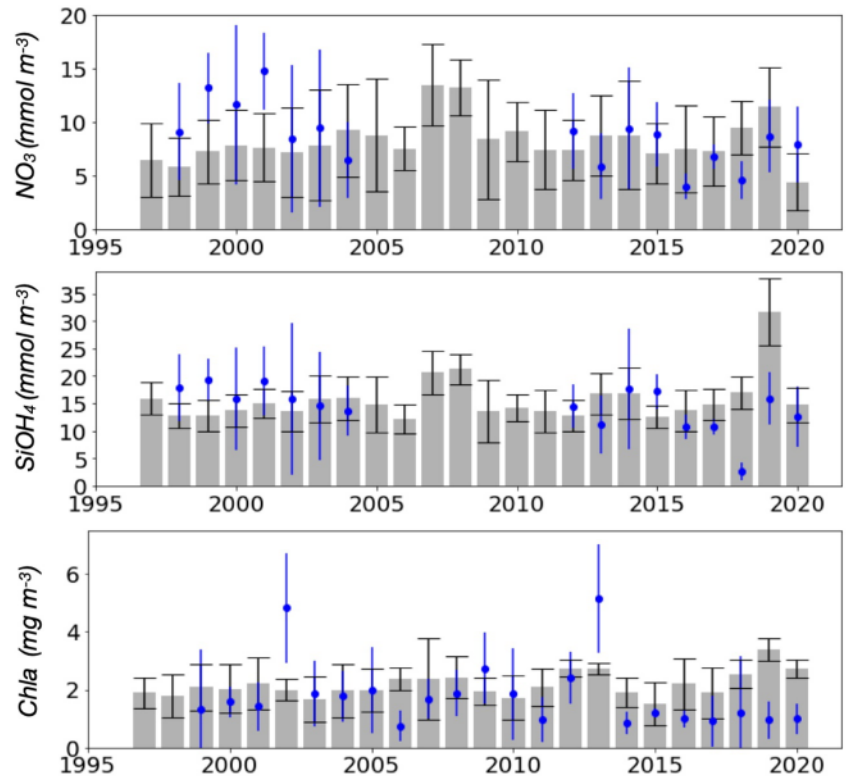

Figure 5. Simulated (gray bars) and observed (blue symbols) nitrate and silicate concentrations in spring (average April-May) along GAK1 to GAK7 near the surface (0–10m), and Chl concentrations in spring (average April-May) along GAK1 to GAK7 averaged over 0–50 m. Standard deviations (black for the model and blue lines for observations) represent the combined variability within the spring (April and May) and along the Seward Line.

3.2.2. EOF Analysis for Springtime

Mode 1 indicates that 26% of the simulated interannual springtime variance is associated with a coherent response across all zooplankton functional groups (except ZS2). The temporal amplitude of the mode is predominantly positive during 1996–2006, 2009–2011 and 2017–2018 and negative during 2007–2008 and 2012–2016 (Figure 8). When regressed independently against each variable, mode 1 explains high percentages (54%–81%) of the interannual springtime variance of all zooplankton except ZS2, and with biomasses all varying in phase with the temporal amplitude of the mode. The amplitude of mode 1 is also strongly correlated with the wintertime (January-February) variability of the variables that emerged as leading contributors for this mode, namely: ZS1 ($r = 0.71$, $p \leq 0.05$), ZL1 ($r = 0.54$, $p \leq 0.05$), ZL2_3 ($r = 0.58$, $p \leq 0.05$), and ZP ($r = 0.63$, $p \leq 0.05$), indicating carry-over effects from the previous year.

Mode 2 indicates that 21% of the simulated interannual springtime variance is associated with a strong response of diatoms to macronutrients (nitrate and silicate) availability, and a more moderate response of ZL1 and ZL2_3 to diatom availability. The temporal amplitude of the mode is predominantly positive during 2005–2014 and 2018–2020, and negative during 1996–2004 and 2015–2017 (Figure 8). When regressed independently against each variable, mode 2 explains high percentages (48%–65%) of the interannual springtime variance for NO_3, $SiOH_4$, and diatoms and moderate percentages (20%–33%) of the interannual springtime variance for MLD, dFe, ZL1, and ZL2_3. While NO_3, $SiOH_4$, diatoms, ZL1, and ZL2_3 all vary in phase with the temporal amplitude of the mode, dFe concentrations vary out-of-phase, suggesting that years with high macronutrients and diatoms have lower dFe concentrations and that iron does not have a limiting effect (at least compared to that of nitrate) on diatom growth during spring. The amplitude of mode 2 is also strongly correlated with the wintertime (January-February) variability of NO_3 ($r = 0.75$, $p \leq 0.05$) and $SiOH_4$ ($r = 0.79$, $p \leq 0.05$), thereby indicating that springtime macronutrient availability is primarily determined by wintertime conditions. Additionally, the wintertime variability of NO_3 and $SiOH_4$ over the shelf is strongly correlated to their wintertime variability over

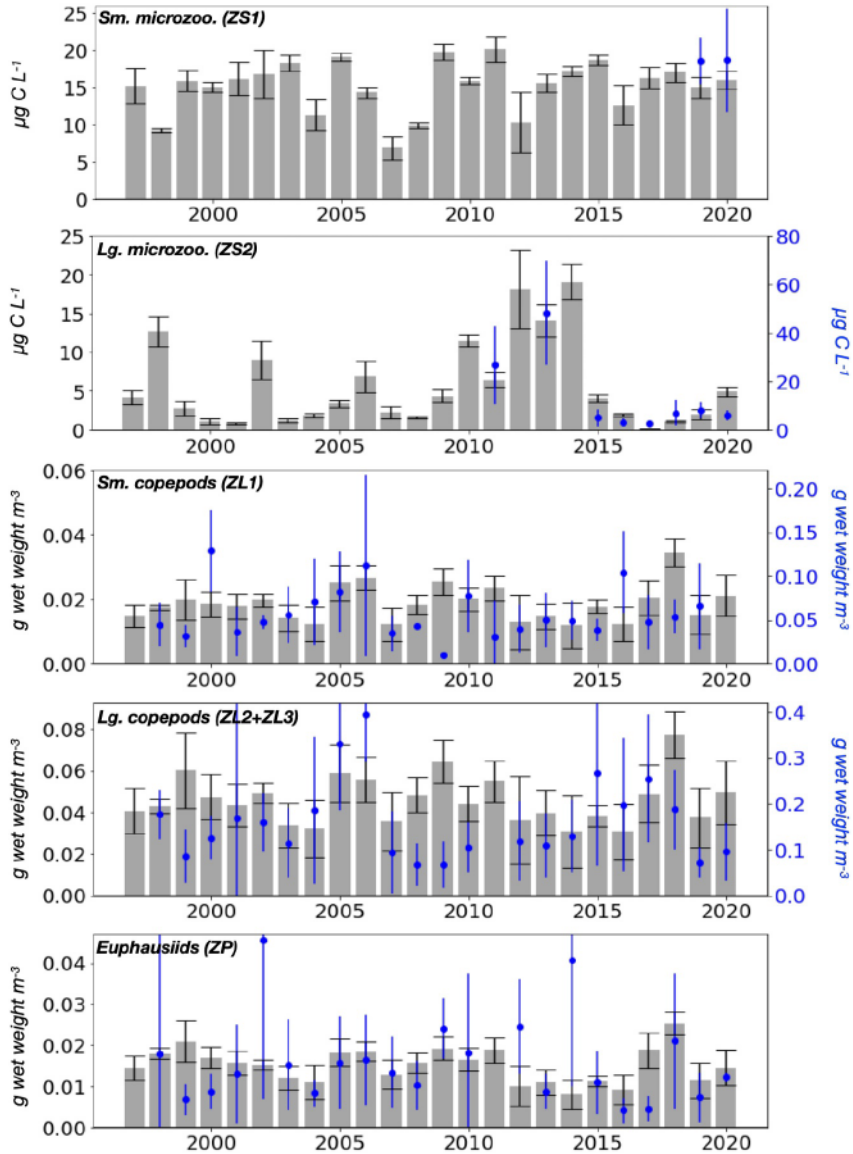

Figure 6. Simulated (gray bars) and observed (blue symbols) small and large microzooplankton in May along GAK1 to GAK7 near the surface (0–10 m) and small and large copepods and euphausiids biomass in spring (average April-May) along GAK1 to GAK7 averaged over 0–100 m. Standard deviations (black for the model and blue lines for observations) represent the spatial variability. For small microzooplankton and euphausiids, observed and simulated biomass are on the same *y*-axis. For large microzooplankton, small and large copepods, simulated biomass is given on the left *y*-axis in black and observed biomass is on the right *y*-axis in blue.

the offshore region of the model domain ($r = 0.85$, $p \leq 0.05$ for NO_3 and $r = 0.70$, $p \leq 0.05$ for $SiOH_4$), meaning that the simulated springtime variability of macronutrients on the shelf is closely tied to the wintertime concentrations offshore. Furthermore, wintertime macronutrients variability over the offshore region is positively correlated to the annual variability in upper water column salinity ($r = 0.61$, $p \leq 0.05$ for NO_3 and $r = 0.59$, $p \leq 0.05$ for $SiOH_4$) and negatively correlated to the annual variability in SSH ($r = -0.53$, $p \leq 0.05$ for NO_3 and $r = -0.49$, $p \leq 0.05$ for $SiOH_4$). The wintertime nitrate variability over the offshore region is also negatively correlated to the PDO index ($r = -0.53$, $p \leq 0.05$). Times series for these variables are shown in Figure S4 in Supporting Information S1.

Mode 3 indicates that 15% of the simulated interannual springtime variance is associated with a strong response of nanophytoplankton to light availability (i.e., PAR), and to a more moderate response of ZS1 and ZS2 to

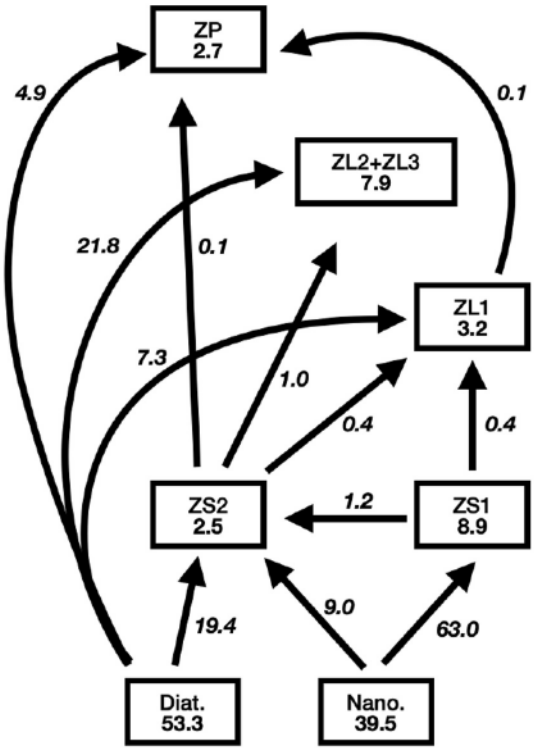

Figure 7. Mean biomasses and grazing fluxes integrated (mmol N m^{-2}) over March to May and the upper 50 m of the NGA shelf water column. ZS1: small microzooplankton, ZS2: large microzooplankton, ZL1: small copepods, ZL2 + ZL3: large copepods, ZP: euphausiids.

nanophytoplankton availability. The temporal amplitude of the mode is predominantly positive during 2010–2015 and negative during 1998–1999, 2004–2008, and 2018–2020 (Figure 8). When regressed independently against each variable, mode 3 explains high percentages (49%–69%) of the interannual springtime variance for PAR and nanophytoplankton and moderate percentages (19%–25%) of the interannual springtime variance for NH_4, ZS1, and ZS2. Springtime PAR, NH_4, nanophytoplankton, ZS1 and ZS2 all vary in phase with the temporal amplitude of the mode.

3.3. Interannual Summertime Variability

3.3.1. Mean Summertime Biomasses and Grazing Fluxes

The mean cumulated nanophytoplankton biomass during summer (Figure 9) is twice as high as the biomass of diatoms. As in springtime, nanophytoplankton is mainly consumed by ZS1 (but with a flux 3 times as high as the flux from nanophytoplankton to ZS2). While diatoms are the main food source for ZL1, ZL2_3 and ZP during spring (consuming ~5 times as much diatoms as their other preys), nanophytoplankton becomes the main food source for ZS2 during summer (consuming 50% more nanophytoplankton than diatoms). ZL1 consumes ZS1 and ZS2 in same amounts and ZP consumes ZS2 and ZL1 in same amounts.

3.3.2. EOF Analysis for Summertime

Mode 1 indicates that 36% of the simulated interannual summertime variance is associated with a strong response of diatoms to macronutrient (nitrate and ammonium) availability, and subsequently mesozooplankton in response to diatoms availability. The temporal amplitude of the mode is predominantly positive during 2003–2005, 2007–2010 and 2018–2019 and negative during 1996–1999 and 2012–2016 (Figure 10). When regressed independently against each variable, mode 1 explains high percentages (50%–89%) of the interannual summertime variance for NO_3, NH_4, diatoms, ZL1, ZL2_3, and ZP. Summertime NO_3, NH_4, diatoms, ZL1, ZL2_3, and ZP all vary in phase with the temporal amplitude of the mode. The amplitude of mode 1 is also strongly correlated with the springtime EOF mode 2 ($r = 0.69, p \leq 0.05$) accounting for 48% of springtime diatoms variability, suggesting that diatoms variability during summer is partly explained by springtime conditions.

Mode 2 indicates that 27% of the simulated interannual summertime variance is associated with a strong response of nitrate, nanophytoplankton, and microzooplankton biomasses. The temporal amplitude of the mode is predominantly positive during 2007–2014 and negative during 1996–2006 and 2017–2020 (Figure 10). When regressed independently against each variable, mode 2 explains high percentages (40%–78%) of the summertime variance for NO_3, nanophytoplankton, ZS1, and ZS2. While summertime NO_3, nanophytoplankton, and ZS2 biomasses all vary in-phase with the temporal amplitude of the mode, summertime ZS1 biomass varies out-of-phase. The strong response of nitrate, nanophytoplankton, and microzooplankton during summer is presumably associated with nitrogen limitation on nanophytoplankton growth, and either a competitive (ZS2 over ZS1) or top-down (ZS2 on ZS1) effect for microzooplankton since ZS1 and ZS2 vary in opposite directions (i.e., higher availability of nanophytoplankton coincides with an increase in ZS2 and decrease in ZS1). The amplitude of mode 2 is uncorrelated with the springtime EOF mode 3 ($r = -0.12$, $p = 0.57$), which suggests that summertime nanophytoplankton variability is not strongly dependent on springtime conditions.

Mode 3 indicates that 19% of the simulated interannual summertime variance is characterized by a strong signal in abiotic variables (higher PAR and temperature, and shallower MLD), but without a covarying biotic response. The temporal amplitude of the mode is predominantly positive during 2002–2005 and 2014–2016 and negative during 1999–2001 and 2006–2012 (Figure 10). When regressed independently against each variable, mode 3 explains high percentages (45%–76%) of the interannual summertime variance for PAR, temperature, and MLD.

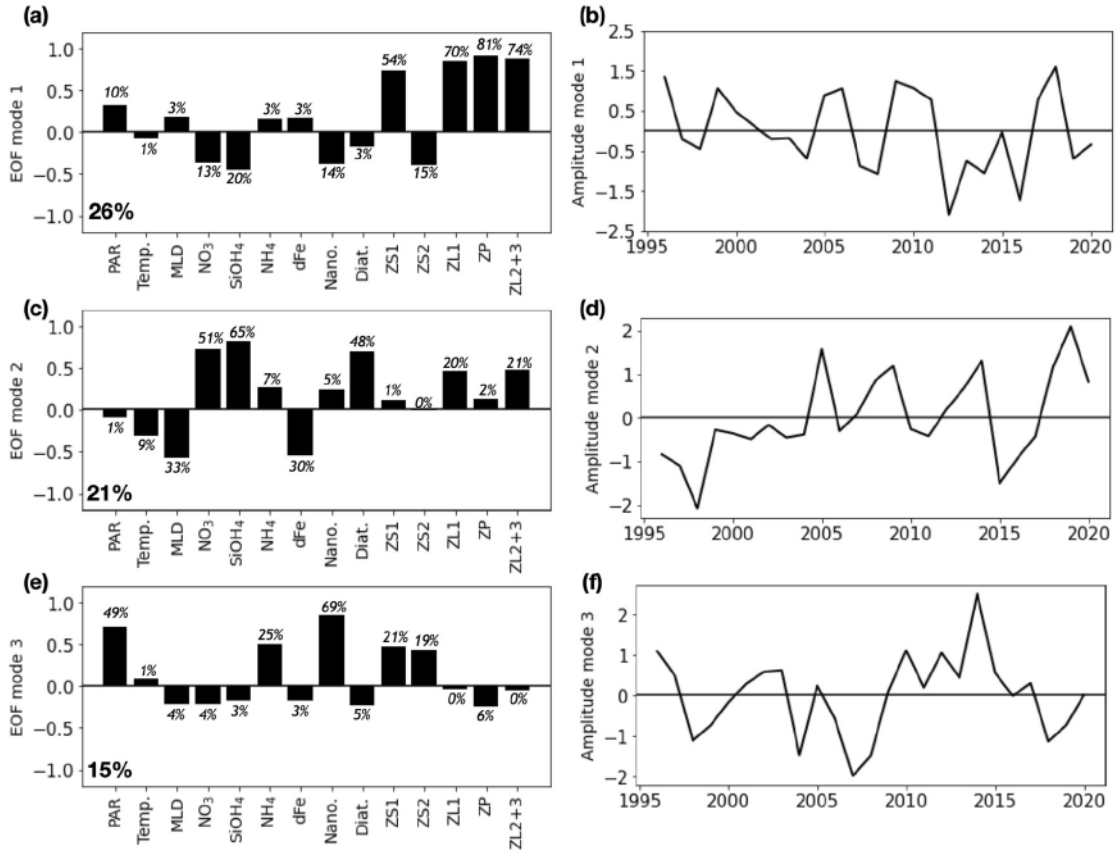

Figure 8. Empirical orthogonal functions (EOF) for combined variables: PAR, temperature, MLD, nutrients, and all planktonic functional groups in spring. Panels (a), (c) and (e) present the EOF values for each variable respectively for the modes 1, 2 and 3, with the percentages of total variance contributed by each mode indicated in the lower left corners. Panels (b), (d) and (f) present the EOF temporal amplitudes respectively for the modes 1, 2 and 3. Values in italic in (a), (c), and (e) indicate the percentages of the interannual springtime variance for each variable explained by the temporal amplitude of each mode. ZS1: small microzooplankton, ZS2: large microzooplankton, ZL1: small copepods, ZL2 + ZL3: large copepods, ZP: euphausiids.

As expected, summertime PAR and temperature vary in phase with the temporal amplitude of the mode, while summertime MLD varies out-of-phase (i.e., higher surface warming associated with incoming solar radiation results in a shallower mixed layer depth).

3.4. Interannual Changes in Energy Transfers

Over the entire season (March-September), the ratio of diatom biomass to total phytoplankton biomass (hereafter referred to as D/(N + D)) is on average 0.52, meaning that for an "average" year there is nearly as much nanophytoplankton as diatoms. Nanophytoplankton is the main food source for ZS1, and diatoms are the main food source for ZS2, ZL1, ZL2_3 and ZP. ZL1 consume ZS1 and ZS2 in comparable amounts and ZP consume ZS2 and ZL1 in equivalent amounts (Figure 11).

Years with low nitrate concentrations (1996, 2003, 2006, 2011, and 2015–2017) have on average 14% less nitrate over March to September than an average year. Low nitrate years exhibit a reduction (by ~5%) in both diatom and nanophytoplankton biomass with no change in the phytoplankton community composition (D/(N + D) changes by only −0.2%) (Figure 12). All zooplankton decline except ZS1, either due to a relaxation of the top-down pressure of ZS2 on ZS1 (as both ZS2 and the grazing flux from ZS2 to ZS1 are reduced) or to a competitive advantage of ZS1 over ZS2 for nanophytoplankton (grazing flux from nanophytoplankton to ZS1 is increased whereas the grazing flux from nanophytoplankton to ZS2 is reduced). Under low nitrate conditions, ZL1 and ZL2_3 are reduced by ~3% and ZP is virtually unaffected (<1% reduction). ZS2 is the most sensitive plankton group and decreases by ~20%. Grazing fluxes on both diatoms and ZS2 decrease, while the grazing flux of ZL1

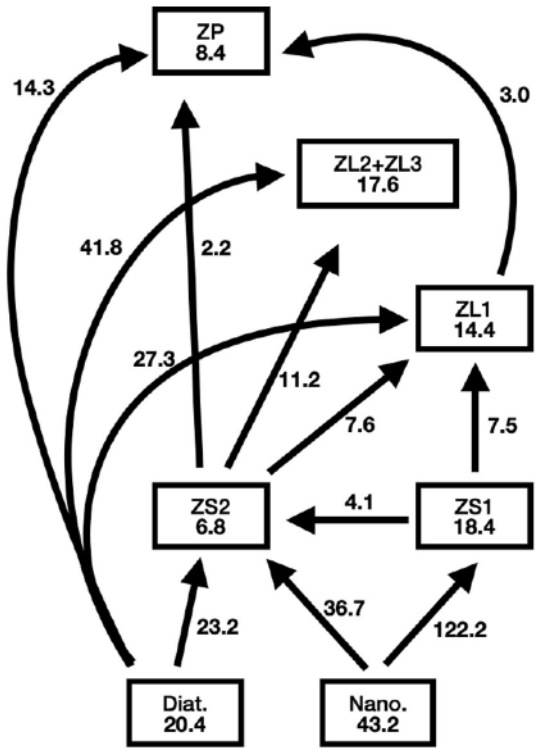

Figure 9. Mean biomasses and grazing fluxes integrated (mmol N m^{-2}) over July to September and the upper 50 m of the NGA shelf water column. ZS1: small microzooplankton, ZS2: large microzooplankton, ZL1: small copepods, ZL2 + ZL3: large copepods, ZP: euphausiids.

on ZS1 increases. In contrast, years with high nitrate concentrations (2004–2005, 2007–2010, 2012–2014 and 2018–2019) have on average 15.2% more nitrate and changes carry opposite signs but comparable amplitudes relative to those described for low nitrate conditions. All planktonic groups and grazing fluxes increase, except for ZS1 biomass, ZS1 grazing on nanophytoplankton, and ZL1 grazing on ZS1.

Years with low relative diatom abundance (i.e., low D/(N + D) ratios in1996–1998, 2001–2003 and 2010–2016) are characterized by a ~11% reduction in diatoms and 4.5% increase in nanophytoplankton. While ZS2 increases (as well as all grazing fluxes toward ZS2), ZS1 and its grazing flux on nanophytoplankton decrease. All grazing fluxes of mesozooplankton on diatoms decrease and although all grazing fluxes of mesozooplankton on ZS2 increase, biomasses of all mesozooplankton decrease. In contrast, changes associated with years having high D/(N + D) ratios (1999–2000, 2004–2009 and 2017–2020) all have opposite sign to those during years with low D/(N + D) ratios, but comparable magnitudes: 11.8% increase in diatoms and 4.8% decrease in nanophytoplankton, with a decrease in ZS2 biomass presumably due to lower nanophytoplankton availability. While all grazing fluxes of mesozooplankton on ZS2 decrease, all grazing fluxes of mesozooplankton on diatoms increase and all mesozooplankton biomasses increase. As for low/high nitrate conditions, ZS2 is the most sensitive plankton group and changes by ~25% compared to ~10% or less for all the other groups. However, mesozooplankton biomass is more sensitive to changes in D/(N + D) than to changes in nitrate, as evidenced by the almost 20% variation in ZP biomass between years of high and low relative diatom abundances. It is also worth mentioning that years with low and high D/(N + D) ratios do not have noticeable differences in nitrate concentration (−1.9% vs. +2.0% respectively for years with low and high D/(N + D) ratios).

4. Discussion

4.1. Model Evaluation

The model generally reproduces water column properties of observed nitrate, silicate and Chl concentrations on a seasonal timescale, but tends to overestimate silicate concentrations during late summer and fall nearshore (stations GAK 1–2). While simulated nitrate and silicate concentrations (and therefore their utilization) are in agreement with in situ values, the intensity of the spring bloom (in terms of Chl concentration) is slightly higher than observed, which could be due to the parameterization of the carbon-to-chlorophyll ratio in the model. It is also worth noting that the timing of field cruises does not always coincide with the spring Chl peak, which would result in an apparent lowering the actual spring bloom intensity. For zooplankton, the model reproduces the order of magnitude of observed biomasses when considering monthly climatological values. Whereas in situ data for microzooplankton are too scarce to provide a meaningful evaluation, the model correctly predicts the seasonality and peak occurrences of small copepods (summer), large copepods (spring), and euphausiids (late summer/fall). However, simulated values tend to underestimate small copepod biomass during summer and large copepod biomass during spring. The simulated peak in large copepod biomass occurs a month later than that observed (i.e., June instead of May). While observations exhibit substantial year-to-year variability during these months, model-data discrepancies are more likely associated with uncertainty in the parameterization of grazing rate and prey preferences, as well as an oversimplified representation of diapause (simulated ZL3 biomass is set to zero every year in early July, whereas large copepods have been observed to start diapausing progressively in June through summer). Understanding the effect of diapause variability on the seasonality of ZL3 should be further examined in future model experiments.

Simulated fields were also evaluated in terms of their interannual variability averaged during spring and along the Seward Line. Such comparisons are inherently challenging as observations are not have been collected at the same time every year relative to the timing of the bloom and include substantial variability across stations. Furthermore,

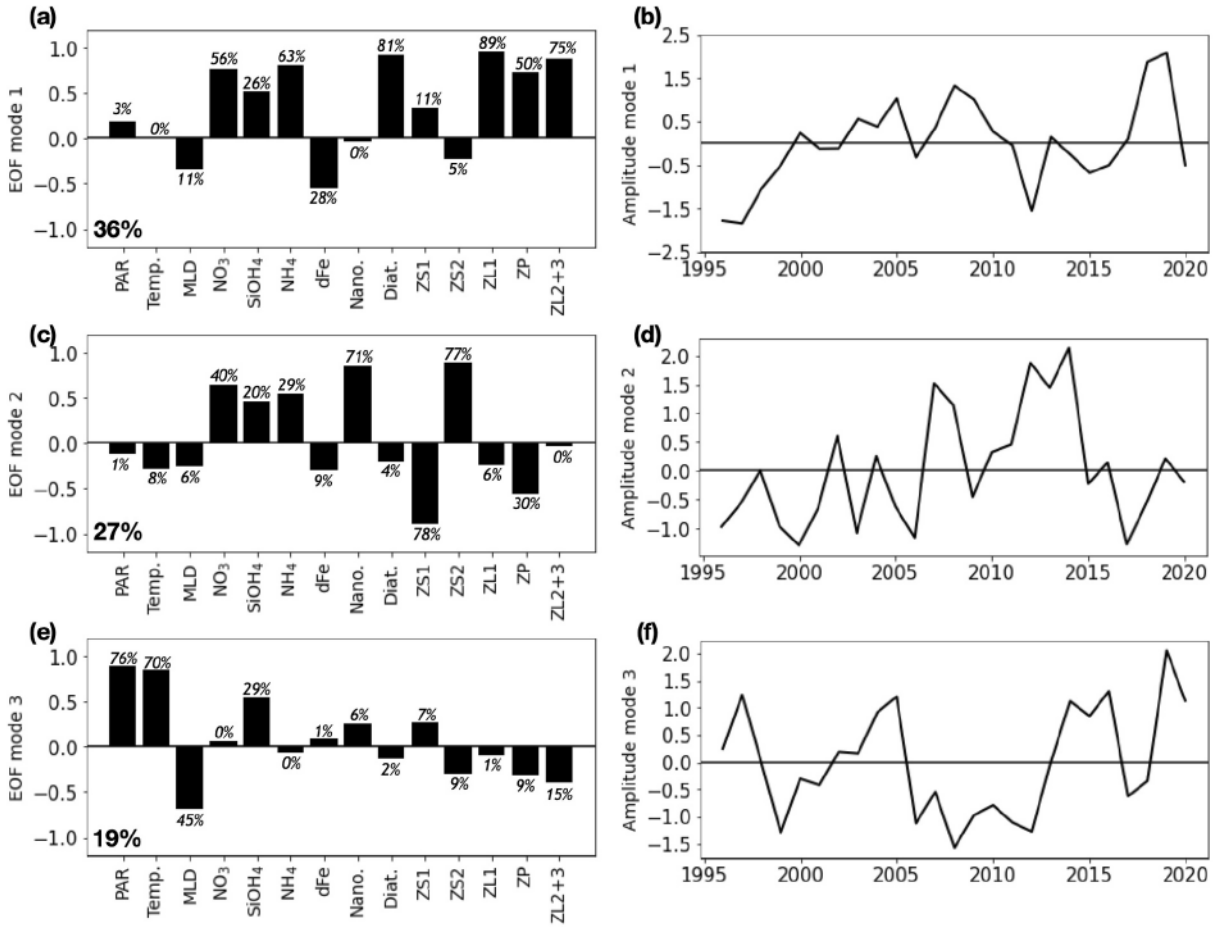

Figure 10. Empirical orthogonal functions (EOF) for combined variables: PAR, temperature, MLD, nutrients, and all planktonic functional groups in summer. Panels (a), (c), and (e) present the EOF values for each variable respectively for the modes 1, 2 and 3, with the percentages of total variance contributed by each mode indicated in the lower left corners. Panels (b), (d), and (f) present the EOF temporal amplitudes respectively for the modes 1, 2, and 3. Values in italic in (a), (c), and (e) indicate the percentages of the interannual summertime variance for each variable explained by the temporal amplitude of each mode. ZS1: small microzooplankton, ZS2: large microzooplankton, ZL1: small copepods, ZL2 + ZL3: large copepods, ZP: euphausiids.

since the model does not include data assimilation, simulated and observed variables will likely have limited agreement for years when shelf waters are strongly influence by eddy activity that may exist either in the model or in nature. For nutrients and microzooplankton, evaluating interannual variability is also limited because extended periods lack observations, especially from late fall through early spring. While the model generally captures the period of lower large microzooplankton biomass observed since 2015 relative to 2011–2013, having the ability to perform additional evaluation of the microzooplankton groups would greatly help interpret ecosystem linkages between simulated phytoplankton and mesozooplankton responses. Simulated Chl concentrations generally agree with the dominant observed patterns, including the decline in Chl concentrations during the 2014-2016 Marine Heat Wave (MHW). In the model, the reduced Chl concentrations during the MHW are primarily associated with a significant decrease in diatom biomass (Figure S1 in Supporting Information S1), which is consistent with reported changes in the observed phytoplankton community structure (Batten et al., 2018, 2022; Strom et al., 2023a). For euphausiids, the model reproduces the significantly lower biomass observed during the peak of the MHW in 2015–2016 (Strom et al., 2023a). While the simulation reproduces the dominant observed patterns for small copepods, it does not fully account for the interannual variability of large copepods. In particular, existing studies for the NGA have highlighted a relationship between copepod abundances and temperature (Kimmel & Duffy-Anderson, 2020; Litzow et al., 2020; Sousa et al., 2016), including increased abundances during the 2014–2016 MHW (Batten et al., 2022; Kimmel & Duffy-Anderson, 2020; Litzow et al., 2020). Hence, the importance of temperature as a driver of copepod interannual variability may not be sufficiently emphasized in the current model formulation and parameterization (see section "Zooplankton dynamic" below). The simulation

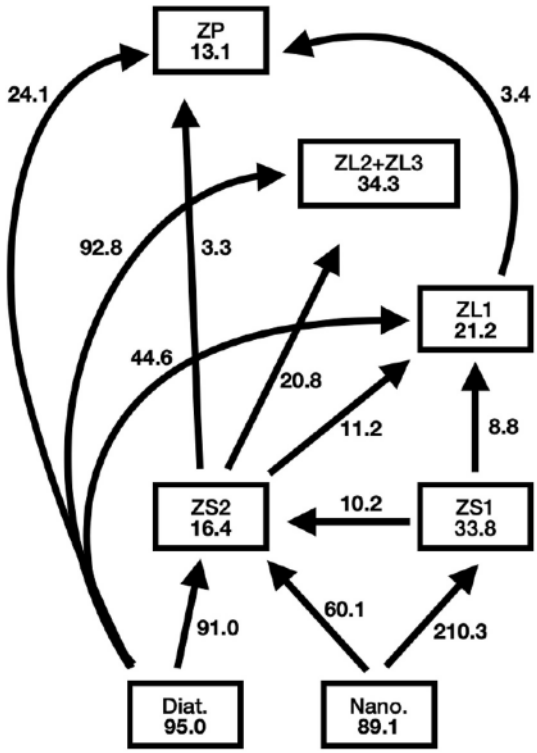

Figure 11. Mean biomasses and grazing fluxes integrated (mmol N m^{-2}) over March to September and the upper 50 m of the NGA shelf water column. ZS1: small microzooplankton, ZS2: large microzooplankton, ZL1: small copepods, ZL2 + ZL3: large copepods, ZP: euphausiids.

may also lack important top-down controls by higher trophic level species, that could have been relaxed during the 2014–2016 MHW (Batten et al., 2022) as populations of forage fish, such as capelin, sand lance, and herring, dramatically declined (Arimitsu et al., 2021).

While the model evaluation focused on the Seward Line, abiotic and biotic properties at stations GAK1-GAK7 (see Figure 2) are expected to be representative of the main oceanographic regimes in the coastal NGA (inner shelf dominated by freshwater input, mid-shelf dominated by Alaska Coastal Current, and outer shelf dominated by eddies) and should provide a robust evaluation of the nutrient and plankton dynamics expected regionally over the shelf. However, future model analysis focusing on strongly anomalous areas of the NGA (e.g., Copper River plume) may benefit from additional evaluation of local ecosystem processes. Overall, the seasonal and interannual model evaluation performed here represents an important contribution as it incorporates (and in some respects augments) the necessary levels of planktonic food web complexity and spatial resolution identified in previous modeling studies (e.g., Coyle et al., 2012; Hermann et al., 2009; Hinkley et al., 2009), but also extends the results to a longer simulation period (25 years) allowing a more robust characterization of climate variability and change in the NGA region (akin to the historical simulation of Hauri et al. (2021) for ocean acidification in the Gulf of Alaska).

4.2. Phytoplankton Variability

While the model reproduces the observed diatom-dominated community during spring and nanophytoplankton-dominated community during summer for shelf waters (Aguilar-Islas et al., 2016; Strom et al., 2010), the EOF analysis sheds additional light on the leading modes of springtime and summertime variability of the broader planktonic community and their abiotic and biotic drivers.

4.2.1. Importance of Macronutrients for Springtime Variability in Diatoms

During spring (March-May), diatom and nanophytoplankton responses project on two distinct modes of variability, indicating that their primary dynamics vary independently. The EOF mode associated with diatoms indicates that interannual variability in springtime macronutrients concentration is an important driver of the diatom-dominated spring bloom magnitude, which is consistent with the long-standing hypothesis that nitrate is an important driver of primary production over the shelf (Batchelder et al., 2013; Childers et al., 2005; Coyle et al., 2012; Fiechter & Moore, 2009; Waite & Mueter, 2013). For instance, macronutrients addition experiments indicated nitrogen limitation of phytoplankton growth rates starting in late April and continuing through summer at various locations of the inner and middle shelf (Strom et al., 2006). While silicate does not significantly limit phytoplankton growth over the shelf (Childers et al., 2005; Fiechter & Moore, 2009; Hinckley et al., 2009), its concentration generally covaries with that of nitrate in our analysis because both are replenished by winter downwelling, and both are utilized by diatoms during the spring bloom. The simulated springtime and wintertime variability of shelf macronutrients are also closely related to wintertime concentrations in the offshore region of the model domain, which supports Ekman transport advection of macronutrient-rich surface waters from offshore during winter downwelling conditions as an important mechanism for replenishment of nitrate and silicate over the shelf prior to the spring bloom (Hermann et al., 2009; Weingartner et al., 2005). While various processes are known to enhance nutrient supply to surface waters in the GOA (e.g., Fiechter & Moore, 2009; Hauri et al., 2021), the negative correlation between simulated offshore nitrate concentrations and the Pacific Decadal Oscillation (PDO) index suggests a connection to oceanic and atmospheric process acting at the scale of the GOA basin. Positive phases of the PDO are known to coincide with negative wind stress curl anomalies and reduced Ekman upwelling in the center of the Alaska Gyre (Auad, 2008; Di Lorenzo et al., 2008; Lagerloef, 1995), which would lead to reduced availability in macronutrients near the surface and explain the negative correlation with simulated nitrate concentrations in the offshore region of the model domain. The reverse applies during negative phases of

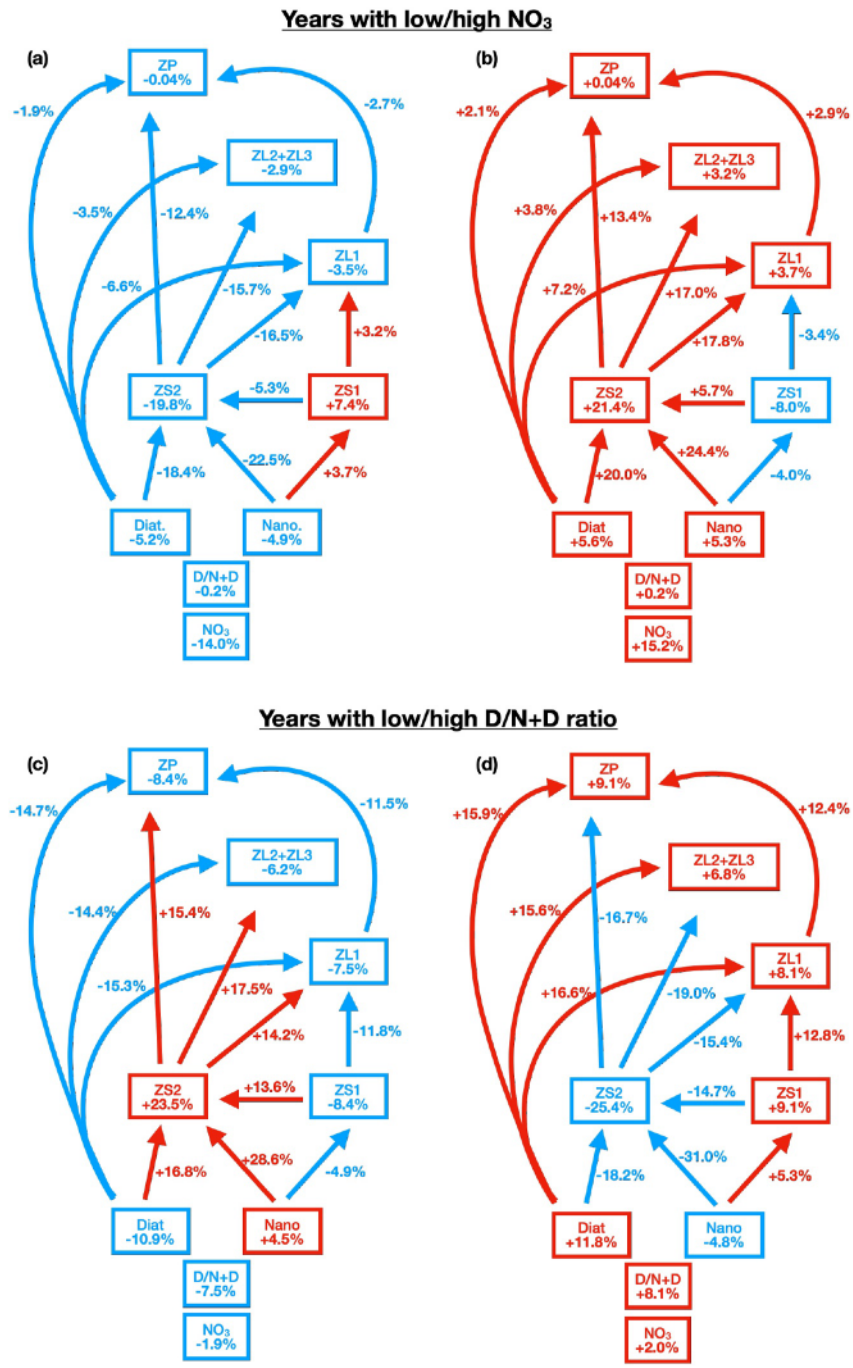

Figure 12. Percentages of interannual change in biomasses and grazing fluxes cumulated over the months of March to September for years with low (a) versus high (b) nitrate concentrations and years with low (c) versus high (d) ratios of diatoms to total phytoplankton biomass (D/(N + D)), relative to the mean biomasses and fluxes presented in Figure 11. A decrease in the percentage is represented in blue and an increase in red. ZS1: small microzooplankton, ZS2: large microzooplankton, ZL1: small copepods, ZL2 + ZL3: large copepods, ZP: euphausiids.

the PDO, whereby the GOA would experience positive wind stress curl, enhanced Ekman upwelling in the center of the Alaska Gyre, and increased macronutrient availability. The connection to the basin scale circulation is confirmed by the negative correlation between simulated nitrate and SSH offshore, which is consistent with the expected positive SSH anomalies in the GOA during positive phases of the PDO (Di Lorenzo et al., 2008). Finally, dFe responding out-of-phase with macronutrients and diatoms in the EOF mode 2 likely results from the

combination of dFe consumption by diatoms and of the advection of macronutrient-rich and iron-poor surface waters from offshore during wintertime.

4.2.2. Importance of PAR Intensity for Springtime Variability in Nanophytoplankton

The EOF mode 3 for spring shows that higher cumulated PAR values result in higher cumulated nanophytoplankton biomass and vice versa. Although it is difficult to establish a direct link with the magnitude or timing of the spring bloom (as lower PAR values could shift the nanophytoplankton peak to June), this mode suggests that surface light intensity is an important determinant of long-term springtime variability in nanophytoplankton biomass. This finding is supported by Waite and Mueter (2013) who found strong positive effects of PAR on spring Chl on both western and eastern shelves based on a 14-year time series of satellite-derived Chl concentrations in the coastal GOA, and by recent autonomous underwater vehicle observations (NGA-LTER unpubl. data). While light is widely recognized as regulating both the timing and magnitude of spring production in the NGA, very few studies have investigated the relationship between light and primary production in the region. How light regulates phytoplankton biomass is complex and depends not only on available PAR at the surface, but also on stratification and light attenuation through the water column (which itself depends on chlorophyll biomass). For instance, while small changes in the parameterization of phytoplankton self-shading in the model may result in minor biomass adjustments in the water column, it is unlikely that they would significantly affect the onset of the spring bloom and, therefore, the PAR-nanophytoplankton relationship identified here. Furthermore, light regulation also relates to the physiology of the phytoplankton community. For example, photosynthesis-irradiance experiments concluded that phytoplankton communities along the Seward line were high-light adapted during summer 2001 (Strom et al., 2010), but low-light adapted on the eastern-shelf during spring of 2011 and 2013 (Strom et al., 2016). Future model developments will be necessary, along with additional laboratory experiments, to simulate photoadaptation more realistically, (e.g., allow for photosynthetic efficiency parameters to vary in time and with environmental conditions).

4.2.3. Importance of Macronutrients for Summertime Variability

During summer (July-Sep), diatom and nanophytoplankton variability also project on separate EOF modes. While both modes are tied to macronutrient availability, the first mode indicates a strong dependence of diatoms to ammonium and nitrate concentrations, while the second mode relates nanophytoplankton dynamics to nitrate concentrations. The importance of ammonium availability for diatoms but not nanophytoplankton may simply reflect the fact that the half saturation constant for ammonium in the model is 3 times higher for diatoms than for nanophytoplankton (0.3 vs. 0.1 mmol N m^{-3}). The strong correlation between the springtime and summertime diatom modes suggests the existence of mechanisms through which conditions during spring can affect diatoms in summer. While this response could be explained by a simple carry-over effect (i.e., more diatoms in spring leads to more diatom in summer), it could also stem from the fact that higher diatom biomass during spring lead to higher micro- and mesozooplankton biomasses (see Figure 12), which would naturally result in higher ammonium concentrations during summer (and hence higher diatom growth) since the main process increasing ammonium in the model is the recycling of DON and PON produced by zooplankton egestion, excretion, and mortality. This latter pathway is further supported in the model by the significant correlation between ammonium concentrations during summer and nitrate concentrations during spring ($r = 0.92$, $p \leq 0.05$).

4.3. Zooplankton Variability

4.3.1. Importance of Carry-Over Effect for Spring Variability

The leading EOF mode for spring indicates that a substantial fraction of the simulated zooplankton variability during March-May is associated with wintertime concentrations, thereby hinting at a carry-over effect from the previous year. However, since most zooplankton groups in the model reach their maximum concentrations in June or later, the impact of spring bloom dynamics on zooplankton abundances may not be fully reflected in the March-May values and, therefore, overemphasize the wintertime zooplankton variability (i.e., carry-over effect) reflected in the leading EOF mode. This hypothesis is further justified when considering that the leading mode for summer clearly identifies positive relationships between diatoms, mesozooplankton, and euphausiid biomasses potentially resulting from spring bloom dynamics (as discussed above under spring and summer EOF modes for diatoms). Nonetheless, the carry-over effect identified in the simulation should not be discounted as a possible

driver of interannual springtime variability for zooplankton. Based on the summer EOF modes, years with more diatoms and less nanophytoplankton during July-September would lead to relatively less large microzooplankton (ZS2) and more small microzooplankton (ZS1), mesozooplankton (ZL1/2/3), and euphausiids (ZP). This response could explain the pattern associated with the EOF mode for spring, assuming that zooplankton losses during the previous fall and winter do not differentially affect the various zooplankton groups (which is likely the case in the model since mortality rates are either held constant or have the same temperature dependence).

4.3.2. Importance of Bottom-Up Effects for Spring and Summer Variability

The EOF analysis suggests that both springtime (in addition to the carry-over effect) and summertime microzooplankton and copepods variability is related to phytoplankton dynamics, with and both small and large microzooplankton responding to nanophytoplankton biomass and copepods responding to diatom biomass. These findings are consistent with simulated energy transfers through the planktonic food web for 1996–2020, whereby nanophytoplankton is entirely consumed by microzooplankton, and diatoms are mainly consumed by mesozooplankton.

4.3.2.1. Microzooplankton Variability Linked to Nanophytoplankton

Summer conditions are distinct from spring conditions in the linked dynamics of nanophytoplankton, small microzooplankton (ZS1), and large microzooplankton (ZS2). During spring, higher availability of nanophytoplankton leads to an increase in both ZS1 and ZS2, suggesting bottom-up effects. Although ZS2 feeds mainly on diatoms during this season, its interannual variability is more closely associated with that of nanophytoplankton, presumably because diatom biomass is never sufficiently low to limit grazing. Alternatively, bottom-up controls of mesozooplankton by diatoms, associated with top-down regulation of ZS2 by mesozooplankton (as evidenced by the out-of-phase response of ZS2 and ZP in EOF mode 3 for spring and EOF mode 2 for summer) may mask an apparent relationship between ZS2 and diatoms in the analysis. Top-down controls on large microzooplankton by mesozooplankton have indeed been hypothesized in the NGA (Dagg et al., 2009; Liu et al., 2008; Strom et al., 2007, 2019), Eastern Bering Sea (Stoecker, Weigel, & Goes, 2014, Stoecker, Weigel, Stockwell, & Lomas, 2014), and Arctic Ocean (Sherr et al., 2003). During summer, higher nanophytoplankton availability results in an increase in large microzooplankton but a decrease in small microzooplankton, indicative of either a competitive (ZS2 over ZS1) or top-down (ZS2 on ZS1) effect. Microzooplankton communities remain overall understudied relative to most metazoan planktonic functional groups (Strom et al., 2019), and additional studies are needed to clarify the nature of the relationships involved (e.g., competition vs. top-down). In agreement with the simulated bottom-up regulation of ZS2 by nanophytoplankton, Strom et al. (2019) demonstrated that the biomass of large microzooplankton reflected springtime phytoplankton abundance when comparing years with reduced (2011) and enhanced (2013) spring bloom intensities. Even so, the representation of microzooplankton in the model, yet limited by data availability, is unable to capture the large diversity of organisms that exist within this trophic level. In particular, considerable diversity is pooled within the ZS2 group. For instance, large ciliates include both strict heterotrophs and chloroplast-retaining (mixotrophic) taxa (Strom, Bright, & Fredrickson, 2023) which all feed on small phytoplankton (Hansen et al., 1994; Rassoulzadegan et al., 1988) and dinoflagellates include large heterotrophic taxa which are important consumers of diatoms (Sherr & Sherr, 2007), large photosynthetic taxa which are of a size comparable to diatoms but consume smaller prey, and small dinoflagellates which prey on bacteria and smaller flagellates (Jeong et al., 2010). As additional field and laboratory data on these organisms become available, future NGA model simulations should benefit from explicitly include mixotrophy and more clearly differentiating between large ciliates and dinoflagellates in the ZS2 group.

4.3.2.2. Mesozooplankton Variability Linked to Diatoms

The strong bottom-up control of diatoms on mesozooplankton in the simulation is likely the cause for the apparent covariability in their interannual dynamics. Bottom-up controls of copepods and euphausiids in the NGA were similarly identified in previous modeling studies (Coyle et al., 2013, 2019) and long-term data analysis. In particular, Sousa et al. (2016) examined spring mesozooplankton abundances and water mass properties in the northern NGA from 1998 to 2009 and suggested that cross-shelf nutrient transport is essential to sustain high zooplankton populations via phytoplankton blooms. Additionally, Batten et al. (2018) found a strong positive correlation between annual diatom abundance and mesozooplankton biomass anomalies from 2000 to 2013.

However, the simulation does not demonstrate a significant relationship between mesozooplankton and temperature, unlike several recent studies that linked an increase in mesozooplankton biomass, especially copepods, with increasing temperatures (Ferriss & Zador, 2022; Kimmel & Duffy-Anderson, 2020; Litzow et al., 2020; Sousa et al., 2016). While this discrepancy could be partly due to how temperature-dependance for growth and mortality is parameterized in the simulation, the hypotheses put forward to explain the observed impact of temperature involve processes not adequately represented by the current model configuration. For instance, warmer years may induce an earlier start in reproduction (Batten et al., 2022), reduced generation times with faster development into the next stages as well as accelerated entry into diapause for the larger copepods (Kimmel & Duffy-Anderson, 2020). Furthermore, the reported increased of small copepod biomass during warm years is partly influenced by advection into the NGA region of more southern species not included in the current model formulation (Litzow et al., 2020; McKinstry & Campbell, 2018; McKinstry et al., 2022; Strom et al., 2023a; Suryan et al., 2021).

4.4. Planktonic Community Structure

Interannual changes in planktonic community structure and energy transfers were quantified by examining years with contrasting nitrate availability and phytoplankton composition. High nitrate years lead to an increase in both diatom and nanophytoplankton biomass, but without significantly impacting phytoplankton composition and with limited effects on the biomass of large copepods (~3% increase) and euphausiids (no change). In contrast, years with relatively high diatom abundance (i.e., high D/(N + D) ratio) are associated with an increase in all mesozooplankton biomasses and that of euphausiids (9% increase). An important difference between high nitrate and high diatom years has to do with energy transfer through the large microzooplankton group (ZS2). During years when diatoms are relatively more abundant, ZS2 biomass decreases significantly, which disproportionally increases the energy flux from diatoms to large mesozooplankton and euphausiids and effectively decreases the average trophic level at which they feed. This shunting does not occur as efficiently during high nitrate years since both diatom and large microzooplankton biomasses concurrently increase. The sensitivity of ZS2 to these two contrasting ecosystem states is higher than for any other planktonic group in the model. While this finding is consistent with the strong interannual variability of observed large ciliate and dinoflagellate biomass, it could also be explained by the central position that this group occupies in the lower trophic level food web (i.e., subjected to multiple bottom-up and top-down controls). While these results are inherently dependent on model formulation (e.g., trophic connections allowed) and parameterization (e.g., prey preferences and vulnerabilities), they nonetheless suggest that the overall planktonic community structure in the NGA may be more sensitive to changes in phytoplankton composition rather than to changes in phytoplankton abundance alone, especially for euphausiids, which are a key link to higher trophic levels. This finding provides additional insight into the drastic declines in euphausiids, and forage fishes observed during the 2014–2016 MHW (Arimitsu et al., 2021; Strom et al., 2023a), as the simulated relative abundance of diatoms (i.e., D/(N + D) ratio) was particularly low during that period (Figure S1 in Supporting Information S1). While factors driving changes in the D/(N + D) ratio need further attention in future work, the EOF analysis suggests that years characterized by a combination of higher macronutrients availability and lower PAR intensity during spring may lead to a dominance of diatoms over nanophytoplankton, and that this dominance would likely extend to summertime.

5. Conclusion

The seasonal and interannual variability of the planktonic community of NGA shelf waters was explored using a 25-year hindcast from a biogeochemical model specifically configured for the region and embedded in a 3-D coastal ocean circulation model.

The main drivers of the springtime (March-May) and summertime (July-September) variability in simulated plankton biomass were identified as light intensity for nanophytoplankton during spring, and macronutrient availability (in particular nitrate) for diatoms during spring and for both diatoms and nanophytoplankton during summer. Nitrate availability during spring (and by extension nitrate and ammonium availability during the summer) is mainly determined by wintertime conditions in the offshore region of the model domain, indicating connections to basin-scale oceanic processes and atmospheric drivers. Zooplankton variability is a combination of carry-over effect (from the previous year) and prey availability (from the current year), with copepods and euphausiids responding to diatoms and microzooplankton responding to nanophytoplankton. The model also suggests that the relative abundance of diatoms to total phytoplankton plays an important role in controlling

biomass production at the large copepod and euphausiid trophic level. By quantifying the combined variability of multiple key planktonic functional groups over a 25-year period, this work lays the foundation for an improved understanding of long-term impacts of climate change on the NGA shelf.

The physical-biogeochemical model framework used here is comparable in resolution and complexity to those used in previous modeling studies for the Gulf of Alaska (e.g., Coyle et al., 2019; Fiechter & Moore, 2009; Hauri et al., 2020; Hinkley et al., 2009). As such, the present findings contribute to shining light on complementary aspects of the complex array of processes modulating ecosystem dynamics in the NGA that would be difficult to understand based solely on in situ and remotely-sensed observations. The model presented here will also enable future in-depth investigations of the planktonic community response to extreme events (e.g., marine heatwaves) that are expected to increase in intensity relative to historic norms. In particular, future work should focus on describing changes in bottom-up and top-down controls on the planktonic food web during the 2014-2016 marine heatwave and, ultimately, how they affected the NGA ecosystem resilience and recovery.

Data Availability Statement

The physical-biogeochemical model output is publicly available through DataONE at https://doi.org/10.24431/rw1k8f0. The in situ observations are publicly available through the DataONE NGA-LTER Data Catalog (https://search.dataone.org/portals/NGALTER/About-the-Data-Catalog).

Acknowledgments
This research was supported by Grant OCE-1656070 from the National Science Foundation Division of Ocean Sciences and is a contribution to the Northern Gulf of Alaska Long-Term Ecological Research Program (NGA LTER). Any opinions, findings, and conclusions or recommendations expressed here are those of the authors and do not necessarily reflect the views of the National Science Foundation. We thank the captains, crews and marine technicians of R/V Sikuliaq, R/V Alpha Helix, R/V Tiglax, R/V Thomas G. Thompson, R/V Island C, R/V Kilo Moana, and R/V Wecoma for the successful Seward Line sampling conducted over 1997–2020, and the many students, scientists, staff and volunteers who helped contributed to data collections. The collection of in situ observations used for model evaluation were supported by AOOS, EVOSTC, NSF, and NPRB. We also thank two anonymous reviewers for the insightful and constructive comments.

References

Aguilar-Islas, A. M., Séguret, M. J. M., Rember, R., Buck, K. N., Proctor, P., Mordy, C. W., & Kachel, N. B. (2016). Temporal variability of reactive iron over the Gulf of Alaska shelf. *Deep Sea Research Part II: Topical Studies in Oceanography*, *132*, 90–106. https://doi.org/10.1016/j.dsr2.2015.05.004

Aita, M. N., Yamanaka, Y., & Kishi, M. J. (2007). Interdecadal variation of the lower trophic ecosystem in the northern Pacific between 1948 and 2002, in a 3-D implementation of the NEMURO model. *Ecological Modelling*, *202*(1–2), 81–94. https://doi.org/10.1016/j.ecolmodel.2006.07.045

Arimitsu, M. L., Piatt, J. F., Hatch, S., Suryan, R. M., Batten, S., Bishop, M. A., et al. (2021). Heatwave-induced synchrony within forage fish portfolio disrupts energy flow to top pelagic predators. *Global Change Biology*, *27*(9), 1859–1878. https://doi.org/10.1111/gcb.15556

Auad, G. (2008). Response of the Gulf of Alaska 3D winter circulation to oceanic climate shifts: Ecosystem implications. *Geophysical Research Letters*, *35*(2), 2007GL031611. https://doi.org/10.1029/2007GL031611

Batchelder, H., Daly, K., Davis, C., Ji, R., Ohman, M., Peterson, W., & Runge, J. (2013). Climate impacts on zooplankton population dynamics in coastal marine ecosystems. *Oceanography*, *26*(4), 34–51. https://doi.org/10.5670/oceanog.2013.74

Batten, S. D., Ostle, C., Hélaouët, P., & Walne, A. W. (2022). Responses of Gulf of Alaska plankton communities to a marine heat wave. *Deep Sea Research Part II: Topical Studies in Oceanography*, *195*, 105002. https://doi.org/10.1016/j.dsr2.2021.105002

Batten, S. D., Raitsos, D. E., Danielson, S., Hopcroft, R., Coyle, K., & McQuatters-Gollop, A. (2018). Interannual variability in lower trophic levels on the Alaskan Shelf. *Deep Sea Research Part II: Topical Studies in Oceanography*, *147*, 58–68. https://doi.org/10.1016/j.dsr2.2017.04.023

Beamer, J. P., Hill, D. F., Arendt, A., & Liston, G. E. (2016). High-resolution modeling of coastal freshwater discharge and glacier mass balance in the Gulf of Alaska watershed. *Water Resources Research*, *52*(5), 3888–3909. https://doi.org/10.1002/2015WR018457

Brown, M. T., Lippiatt, S. M., & Bruland, K. W. (2010). Dissolved aluminum, particulate aluminum, and silicic acid in northern Gulf of Alaska coastal waters: Glacial/riverine inputs and extreme reactivity. *Marine Chemistry*, *122*(1–4), 160–175. https://doi.org/10.1016/j.marchem.2010.04.002

Carnicer, O., Irwin, A. J., & Finkel, Z. V. (2022). Traits influence dinoflagellate C:N:P. *European Journal of Phycology*, *57*(2), 154–165. https://doi.org/10.1080/09670262.2021.1914860

Cheng, W., Hermann, A. J., Coyle, K. O., Dobbins, E. L., Kachel, N. B., & Stabeno, P. J. (2012). Macro- and micro-nutrient flux to a highly productive submarine bank in the Gulf of Alaska: A model-based analysis of daily and interannual variability. *Progress in Oceanography*, *101*(1), 63–77. https://doi.org/10.1016/j.pocean.2012.01.001

Childers, A. R., Whitledge, T. E., & Stockwell, D. A. (2005). Seasonal and interannual variability in the distribution of nutrients and chlorophyll a across the Gulf of Alaska shelf: 1998–2000. *Deep Sea Research Part II: Topical Studies in Oceanography*, *52*(1–2), 193–216. https://doi.org/10.1016/j.dsr2.2004.09.018

Clarke, A., & Peck, L. S. (1991). The physiology of polar marine zooplankton. *Polar Research*, *10*(2), 355–370. https://doi.org/10.3402/polar.v10i2.6752

Cooney, R. T. (1986). The seasonal occurrence of *Neocalanus cristatus, Neocalanus plumchrus*, and *Eucalanus bungii* over the shelf of the northern Gulf of Alaska. *Continental Shelf Research*, *5*, 541–553. https://doi.org/10.1016/0278-4343(86)90075-0

Coyle, K. O., Cheng, W., Hinckley, S. L., Lessard, E. J., Whitledge, T., Hermann, A. J., & Hedstrom, K. (2012). Model and field observations of effects of circulation on the timing and magnitude of nitrate utilization and production on the northern Gulf of Alaska shelf. *Progress in Oceanography*, *103*, 16–41. https://doi.org/10.1016/j.pocean.2012.03.002

Coyle, K. O., Gibson, G. A., Hedstrom, K., Hermann, A. J., & Hopcroft, R. R. (2013). Zooplankton biomass, advection and production on the northern Gulf of Alaska shelf from simulations and field observations. *Journal of Marine Systems*, *128*, 185–207. https://doi.org/10.1016/j.jmarsys.2013.04.018

Coyle, K. O., Hermann, A. J., & Hopcroft, R. R. (2019). Modeled spatial-temporal distribution of productivity, chlorophyll, iron and nitrate on the northern Gulf of Alaska shelf relative to field observations. *Deep Sea Research Part II: Topical Studies in Oceanography*, *165*, 163–191. https://doi.org/10.1016/j.dsr2.2019.05.006

Coyle, K. O., & Pinchuk, A. I. (2003). Annual cycle of zooplankton abundance, biomass and production on the northern Gulf of Alaska shelf, October 1997 through October 2000: Zooplankton on the northern Gulf of Alaska shelf. *Fisheries Oceanography*, *12*(4–5), 327–338. https://doi.org/10.1046/j.1365-2419.2003.00256.x

Coyle, K. O., & Pinchuk, A. I. (2005). Seasonal cross-shelf distribution of major zooplankton taxa on the northern Gulf of Alaska shelf relative to water mass properties, species depth preferences and vertical migration behavior. *Deep Sea Research Part II: Topical Studies in Oceanography*, *52*(1–2), 217–245. https://doi.org/10.1016/j.dsr2.2004.09.025

Crusius, J., Schroth, A. W., Gassó, S., Moy, C. M., Levy, R. C., & Gatica, M. (2011). Glacial flour dust storms in the Gulf of Alaska: Hydrologic and meteorological controls and their importance as a source of bioavailable iron: Glacial flour dust in the Gulf of Alaska. *Geophysical Research Letters*, *38*(6), L06602. https://doi.org/10.1029/2010GL046573

Crusius, J., Schroth, A. W., Resing, J. A., Cullen, J., & Campbell, R. W. (2017). Seasonal and spatial variabilities in northern Gulf of Alaska surface water iron concentrations driven by shelf sediment resuspension, glacial meltwater, a Yakutat eddy, and dust: Variabilities in Gulf of Alaska Fe Sources. *Global Biogeochemical Cycles*, *31*(6), 942–960. https://doi.org/10.1002/2016GB005493

Dagg, M., Strom, S., & Liu, H. (2009). High feeding rates on large particles by *Neocalanus flemingeri* and *N. plumchrus*, and consequences for phytoplankton community structure in the subarctic Pacific Ocean. *Deep Sea Research Part I: Oceanographic Research Papers*, *56*(5), 716–726. https://doi.org/10.1016/j.dsr.2008.12.012

Danielson, S. L., Hill, D. F., Hedstrom, K. S., Beamer, J., & Curchitser, E. (2020). Demonstrating a high-resolution Gulf of Alaska ocean circulation model forced across the coastal interface by high-resolution terrestrial hydrological models. *Journal of Geophysical Research: Oceans*, *125*(8). https://doi.org/10.1029/2019JC015724

Di Lorenzo, E., Schneider, N., Cobb, K. M., Franks, P. J. S., Chhak, K., Miller, A. J., et al. (2008). North Pacific Gyre Oscillation links ocean climate and ecosystem change. *Geophysical Research Letters*, *35*(8), L08607. https://doi.org/10.1029/2007GL032838

Doubleday, A. J., & Hopcroft, R. R. (2015). Interannual patterns during spring and late summer of larvaceans and pteropods in the coastal Gulf of Alaska, and their relationship to pink salmon survival. *Journal of Plankton Research*, *37*(1), 134–150. https://doi.org/10.1093/plankt/fbu092

Ducklow, H., Cimino, M., Dunton, K. H., Fraser, W. R., Hopcroft, R. R., Ji, R., et al. (2022). Marine pelagic ecosystem responses to climate variability and change. *BioScience*, *72*(9), 827–850. https://doi.org/10.1093/biosci/biac050

Egbert, G. D., & Erofeeva, S. Y. (2002). Efficient inverse modeling of barotropic ocean tides. *Journal of Atmospheric and Oceanic Technology*, *19*(2), 183–204. https://doi.org/10.1175/1520-0426(2002)019<0183:EIMOBO>2.0.CO;2

Eppley, R. W. (1972). Temperature and phytoplankton growth in the sea. *Fishery Bulletin*, *70*, 1063–1085.

European Union-Copernicus Marine Service. (2018a). Global ocean biogeochemistry hindcast. https://doi.org/10.48670/MOI-00019

European Union-Copernicus Marine Service. (2018b). Global ocean physics reanalysis. https://doi.org/10.48670/MOI-00021

Ferriss, B. E., & Zador, S. (2022). *Ecosystem status report 2022: Gulf of Alaska, stock assessment and fishery evaluation report*. North Pacific Fishery Management Council. Retrieved from https://apps-afsc.fisheries.noaa.gov/REFM/docs/2022/GOAecosys.pdf

Fiechter, J., & Moore, A. M. (2009). Interannual spring bloom variability and Ekman pumping in the coastal Gulf of Alaska. *Journal of Geophysical Research*, *114*(C6), C06004. https://doi.org/10.1029/2008JC005140

Fiechter, J., & Moore, A. M. (2012). Iron limitation impact on eddy-induced ecosystem variability in the coastal Gulf of Alaska. *Journal of Marine Systems*, *92*, 1–15. https://doi.org/10.1016/j.jmarsys.2011.09.012

Fiechter, J., Moore, A. M., Edwards, C. A., Bruland, K. W., Di Lorenzo, E., Lewis, C. V. W., et al. (2009). Modeling iron limitation of primary production in the coastal Gulf of Alaska. *Deep Sea Research Part II: Topical Studies in Oceanography*, *56*(24), 2503–2519. https://doi.org/10.1016/j.dsr2.2009.02.010

Haidvogel, D. B., Arango, H. G., Hedstrom, K., Beckmann, A., Malanotte-Rizzoli, P., & Shchepetkin, A. F. (2000). Model evaluation experiments in the North Atlantic Basin: Simulations in nonlinear terrain-following coordinates. *Dynamics of Atmospheres and Oceans*, *32*(3–4), 239–281. https://doi.org/10.1016/S0377-0265(00)00049-X

Hansen, B., Bjornsen, P. K., & Hansen, P. J. (1994). The size ratio between planktonic predators and their prey. *Limnology & Oceanography*, *39*(2), 395–403. https://doi.org/10.4319/lo.1994.39.2.0395

Hare, S. R., & Mantua, N. J. (2000). Empirical evidence for North Pacific regime shifts in 1977 and 1989. *Progress in Oceanography*, *47*(2–4), 103–145. https://doi.org/10.1016/S0079-6611(00)00033-1

Hauri, C., Pagès, R., McDonnell, A. M. P., Stuecker, M. F., Danielson, S. L., Hedstrom, K., et al. (2021). Modulation of ocean acidification by decadal climate variability in the Gulf of Alaska. *Communications Earth and Environment*, *2*(1), 191. https://doi.org/10.1038/s43247-021-00254-z

Hauri, C., Schultz, C., Hedstrom, K., Danielson, S., Irving, B., Doney, S. C., et al. (2020). A regional hindcast model simulating ecosystem dynamics, inorganic carbon chemistry, and ocean acidification in the Gulf of Alaska. *Biogeosciences*, *17*(14), 3837–3857. https://doi.org/10.5194/bg-17-3837-2020

Henson, S. A. (2007). Water column stability and spring bloom dynamics in the Gulf of Alaska. *Journal of Marine Research*, *65*(6), 715–736. https://doi.org/10.1357/002224007784219002

Hermann, A. J., Hinckley, S., Dobbins, E. L., Haidvogel, D. B., Bond, N. A., Mordy, C., et al. (2009). Quantifying cross-shelf and vertical nutrient flux in the Coastal Gulf of Alaska with a spatially nested, coupled biophysical model. *Deep Sea Research Part II: Topical Studies in Oceanography*, *56*(24), 2474–2486. https://doi.org/10.1016/j.dsr2.2009.02.008

Hersbach, H., Bell, B., Berrisford, P., Hirahara, S., Horányi, A., Muñoz-Sabater, J., et al. (2020). The ERA5 global reanalysis. *Quarterly Journal of the Royal Meteorological Society*, *146*(730), 1999–2049. https://doi.org/10.1002/qj.3803

Hinckley, S., Coyle, K. O., Gibson, G., Hermann, A. J., & Dobbins, E. L. (2009). A biophysical NPZ model with iron for the Gulf of Alaska: Reproducing the differences between an oceanic HNLC ecosystem and a classical northern temperate shelf ecosystem. *Deep Sea Research Part II: Topical Studies in Oceanography*, *56*(24), 2520–2536. https://doi.org/10.1016/j.dsr2.2009.03.003

Hirst, A. G., Roff, J. C., & Lampitt, R. S. (2003). A synthesis of growth rates in marine epipelagic invertebrate zooplankton. In *Advances in marine biology* (pp. 1–142). Elsevier. https://doi.org/10.1016/S0065-2881(03)44002-9

Hudson, R. J. M., & Morel, F. M. M. (1993). Trace metal transport by marine microorganisms: Implications of metal coordination kinetics. *Deep Sea Research Part I: Oceanographic Research Papers*, *40*(1), 129–150. https://doi.org/10.1016/0967-0637(93)90057-A

Hurst, M. P., & Bruland, K. W. (2007). An investigation into the exchange of iron and zinc between soluble, colloidal, and particulate size-fractions in shelf waters using low-abundance isotopes as tracers in shipboard incubation experiments. *Marine Chemistry*, *103*(3–4), 211–226. https://doi.org/10.1016/j.marchem.2006.07.001

Ito, S., Yoshie, N., Okunishi, T., Ono, T., Okazaki, Y., Kuwata, A., et al. (2010). Application of an automatic approach to calibrate the NEMURO nutrient–phytoplankton–zooplankton food web model in the Oyashio region. *Progress in Oceanography*, *87*(1–4), 186–200. https://doi.org/10.1016/j.pocean.2010.08.004

Jackson, T., Sathyendranath, S., & Platt, T. (2017). An exact solution for modeling photoacclimation of the carbon-to-chlorophyll ratio in phytoplankton. *Frontiers in Marine Science*, *4*, 283. https://doi.org/10.3389/fmars.2017.00283

Jeong, H. J., Yoo, Y. D., Kim, J. S., Seong, K. A., Kang, N. S., & Kim, T. H. (2010). Growth, feeding and ecological roles of the mixotrophic and heterotrophic dinoflagellates in marine planktonic food webs. *Ocean Science Journal*, *45*(2), 65–91. https://doi.org/10.1007/s12601-010-0007-2

Kilduff, D. P., Di Lorenzo, E., Botsford, L. W., & Teo, S. L. H. (2015). Changing central Pacific El Niños reduce stability of North American salmon survival rates. *Proceedings of the National Academy of Sciences of the United States of America*, *112*(35), 10962–10966. https://doi.org/10.1073/pnas.1503190112

Kimmel, D. G., & Duffy-Anderson, J. T. (2020). Zooplankton abundance trends and patterns in Shelikof Strait, western Gulf of Alaska, USA, 1990–2017. *Journal of Plankton Research*, *42*(3), 334–354. https://doi.org/10.1093/plankt/fbaa019

Kishi, M. J., Kashiwai, M., Ware, D. M., Megrey, B. A., Eslinger, D. L., Werner, F. E., et al. (2007). NEMURO- a lower trophic level model for the North Pacific marine ecosystem. *Ecological Modelling*, *202*(1–2), 12–25. https://doi.org/10.1016/j.ecolmodel.2006.08.021

Ladd, C., Stabeno, P., & Cokelet, E. D. (2005). A note on cross-shelf exchange in the northern Gulf of Alaska. *Deep Sea Research Part II: Topical Studies in Oceanography*, *52*(5–6), 667–679. https://doi.org/10.1016/j.dsr2.2004.12.022

Lagerloef, G. S. (1995). Interdecadal variations in the Alaska Gyre. *Journal of Physical Oceanography*, *25*(10), 2242–2258. https://doi.org/10.1175/1520-0485(1995)025<2242:ivitag>2.0.co;2

Lippiatt, S. M., Lohan, M. C., & Bruland, K. W. (2010). The distribution of reactive iron in northern Gulf of Alaska coastal waters. *Marine Chemistry*, *121*(1–4), 187–199. https://doi.org/10.1016/j.marchem.2010.04.007

Litzow, M. A., Hunsicker, M. E., Ward, E. J., Anderson, S. C., Gao, J., Zador, S. G., et al. (2020). Evaluating ecosystem change as Gulf of Alaska temperature exceeds the limits of preindustrial variability. *Progress in Oceanography*, *186*, 102393. https://doi.org/10.1016/j.pocean.2020.102393

Litzow, M. A., & Mueter, F. J. (2014). Assessing the ecological importance of climate regime shifts: An approach from the North Pacific Ocean. *Progress in Oceanography*, *120*, 110–119. https://doi.org/10.1016/j.pocean.2013.08.003

Liu, H., Dagg, M. J., Napp, J. M., & Sato, R. (2008). Mesozooplankton grazing in the coastal Gulf of Alaska: *Neocalanus* spp. vs. other mesozooplankton. *ICES Journal of Marine Science*, *65*(3), 351–360. https://doi.org/10.1093/icesjms/fsm175

Liu, H., Dagg, M. J., & Strom, S. (2005). Grazing by the calanoid copepod Neocalanus cristatus on the microbial food web in the coastal Gulf of Alaska. *Journal of Plankton Research*, *27*(7), 647–662. https://doi.org/10.1093/plankt/fbi039

Mantua, N. J., Hare, S. R., Zhang, Y., Wallace, J. M., & Francis, R. C. (1997). A Pacific Interdecadal Climate Oscillation with Impacts on Salmon Production. *Bulletin America Meteorology Social*, *78*(6), 1069–1079. https://doi.org/10.1175/1520-0477(1997)078<1069:APICOW>2.0.CO;2

McKinstry, C. A. E., & Campbell, R. W. (2018). Seasonal variation of zooplankton abundance and community structure in Prince William Sound, Alaska, 2009–2016. *Deep Sea Research Part II: Topical Studies in Oceanography*, *147*, 69–78. https://doi.org/10.1016/j.dsr2.2017.08.016

McKinstry, C. A. E., Campbell, R. W., & Holderied, K. (2022). Influence of the 2014–2016 marine heatwave on seasonal zooplankton community structure and abundance in the lower Cook Inlet, Alaska. *Deep Sea Research Part II: Topical Studies in Oceanography*, *195*, 105012. https://doi.org/10.1016/j.dsr2.2021.105012

Megrey, B. A., Rose, K. A., Klumb, R. A., Hay, D. E., Werner, F. E., Eslinger, D. L., & Smith, S. L. (2007). A bioenergetics-based population dynamics model of Pacific herring (*Clupea harengus pallasi*) coupled to a lower trophic level nutrient–phytoplankton–zooplankton model: Description, calibration, and sensitivity analysis. *Ecological Modelling*, *202*(1–2), 144–164. https://doi.org/10.1016/j.ecolmodel.2006.08.020

Mordy, C. W., Stabeno, P. J., Kachel, N. B., Kachel, D., Ladd, C., Zimmermann, M., et al. (2019). Patterns of flow in the canyons of the northern Gulf of Alaska. *Deep Sea Research Part II: Topical Studies in Oceanography*, *165*, 203–220. https://doi.org/10.1016/j.dsr2.2019.03.009

Morel, A., & Maritorena, S. (2001). Bio-optical properties of oceanic waters: A reappraisal. *Journal of Geophysical Research*, *106*(C4), 7163–7180. https://doi.org/10.1029/2000JC000319

Okkonen, S. R., Weingartner, T. J., Danielson, S. L., Musgrave, D. L., & Schmidt, G. M. (2003). Satellite and hydrographic observations of eddy-induced shelf-slope exchange in the northwestern Gulf of Alaska. *Journal of Geophysical Research*, *108*(C2), 2002JC001342. https://doi.org/10.1029/2002JC001342

Peña, M. A., Fine, I., & Callendar, W. (2019). Interannual variability in primary production and shelf-offshore transport of nutrients along the northeast Pacific Ocean margin. *Deep Sea Research Part II: Topical Studies in Oceanography*, *169–170*, 104637. https://doi.org/10.1016/j.dsr2.2019.104637

Peterson, W. T., & Schwing, F. B. (2003). A new climate regime in northeast pacific ecosystems. *Geophysical Research Letters*, *30*(17), 1896. https://doi.org/10.1029/2003GL017528

Pinchuk, A. I., Coyle, K. O., & Hopcroft, R. R. (2008). Climate-related variability in abundance and reproduction of euphausiids in the northern Gulf of Alaska in 1998–2003. *Progress in Oceanography*, *77*(2–3), 203–216. https://doi.org/10.1016/j.pocean.2008.03.012

Rassoulzadegan, F., Laval-Peuto, M., & Sheldon, R. W. (1988). Partitioning of the food ration of marine ciliates between pico- and nanoplankton. *Hydrobiologia*, *159*(1), 75–88. https://doi.org/10.1007/BF00007369

Reed, R. K. (1984). Flow of the Alaskan Stream and its variations. *Deep-Sea Research, Part A: Oceanographic Research Papers*, *31*(4), 369–386. https://doi.org/10.1016/0198-0149(84)90090-6

Rose, J. M., & Caron, D. A. (2007). Does low temperature constrain the growth rates of heterotrophic protists? Evidence and implications for algal blooms in cold waters. *Limnology & Oceanography*, *52*(2), 886–895. https://doi.org/10.4319/lo.2007.52.2.0886

Rose, K. A., Rutherford, E. S., McDermot, D. S., Forney, J. L., & Mills, E. L. (1999). Individual-based model of yellow perch and walleye populations in Oneida lake. *Ecological Monographs*, *69*(2), 127–154. https://doi.org/10.1890/0012-9615(1999)069[0127:IBMOYP]2.0.CO;2

Schmoker, C., Hernández-León, S., & Calbet, A. (2013). Microzooplankton grazing in the oceans: Impacts, data variability, knowledge gaps and future directions. *Journal of Plankton Research*, *35*(4), 691–706. https://doi.org/10.1093/plankt/fbt023

Shchepetkin, A. F., & McWilliams, J. C. (2005). The regional oceanic modeling system (ROMS): A split-explicit, free-surface, topography-following-coordinate oceanic model. *Ocean Modelling*, *9*(4), 347–404. https://doi.org/10.1016/j.ocemod.2004.08.002

Sherr, E., & Sherr, B. (2007). Heterotrophic dinoflagellates: A significant component of microzooplankton biomass and major grazers of diatoms in the sea. *Marine Ecology Progress Series*, *352*, 187–197. https://doi.org/10.3354/meps07161

Sherr, E. B., Sherr, B. F., Wheeler, P. A., & Thompson, K. (2003). Temporal and spatial variation in stocks of autotrophic and heterotrophic microbes in the upper water column of the central Arctic Ocean. *Deep Sea Research Part I: Oceanographic Research Papers*, *50*(5), 557–571. https://doi.org/10.1016/S0967-0637(03)00031-1

Sousa, L., Coyle, K. O., Barry, R. P., Weingartner, T. J., & Hopcroft, R. R. (2016). Climate-related variability in abundance of mesozooplankton in the northern Gulf of Alaska 1998–2009. *Deep Sea Research Part II: Topical Studies in Oceanography*, *132*, 122–135. https://doi.org/10.1016/j.dsr2.2016.04.006

Stabeno, P. J., Bell, S., Cheng, W., Danielson, S., Kachel, N. B., & Mordy, C. W. (2016). Long-term observations of Alaska coastal current in the northern Gulf of Alaska. *Deep Sea Research Part II: Topical Studies in Oceanography*, *132*, 24–40. https://doi.org/10.1016/j.dsr2.2015.12.016

Stabeno, P. J., Bond, N. A., Hermann, A. J., Kachel, N. B., Mordy, C. W., & Overland, J. E. (2004). Meteorology and oceanography of the Northern Gulf of Alaska. *Continental Shelf Research*, *24*(7–8), 859–897. https://doi.org/10.1016/j.csr.2004.02.007

Stoecker, D. K., Weigel, A., & Goes, J. I. (2014). Microzooplankton grazing in the Eastern Bering Sea in summer. *Deep Sea Research Part II: Topical Studies in Oceanography*, *109*, 145–156. https://doi.org/10.1016/j.dsr2.2013.09.017

Stoecker, D. K., Weigel, A. C., Stockwell, D. A., & Lomas, M. W. (2014). Microzooplankton: Abundance, biomass and contribution to chlorophyll in the Eastern Bering Sea in summer. *Deep Sea Research Part II: Topical Studies in Oceanography*, *109*, 134–144. https://doi.org/10.1016/j.dsr2.2013.09.007

Strom, S., Bright, K., & Fredrickson, K. (2023). Widespread ciliate and dinoflagellate mixotrophy may contribute to ecosystem resilience in a subarctic sea: The northern Gulf of Alaska. *Aquatic Microbial Ecology*, *90*, 1–21. https://doi.org/10.3354/ame02005

Strom, S., Macri, E., & Fredrickson, K. (2010). Light limitation of summer primary production in the coastal Gulf of Alaska: Physiological and environmental causes. *Marine Ecology Progress Series*, *402*, 45–57. https://doi.org/10.3354/meps08456

Strom, S., & Northern Gulf of Alaska Long-Term Ecosystem Research Team (2023a). Recent marine heatwaves affect marine ecosystems from Plankton to Seabirds in the Northern Gulf of Alaska. *Oceanography*. https://doi.org/10.5670/oceanog.2023.s1.9

Strom, S., Olson, M., Macri, E., & Mord, C. (2006). Cross-shelf gradients in phytoplankton community structure, nutrient utilization, and growth rate in the coastal Gulf of Alaska. *Marine Ecology Progress Series*, *328*, 75–92. https://doi.org/10.3354/meps328075

Strom, S. L., Fredrickson, K. A., & Bright, K. J. (2016). Spring phytoplankton in the eastern coastal Gulf of Alaska: Photosynthesis and production during high and low bloom years. *Deep Sea Research Part II: Topical Studies in Oceanography*, *132*, 107–121. https://doi.org/10.1016/j.dsr2.2015.05.003

Strom, S. L., Fredrickson, K. A., & Bright, K. J. (2019). Microzooplankton in the coastal Gulf of Alaska: Regional, seasonal and interannual variations. *Deep Sea Research Part II: Topical Studies in Oceanography*, *165*, 192–202. https://doi.org/10.1016/j.dsr2.2018.07.012

Strom, S. L., Macri, E. L., & Olson, M. B. (2007). Microzooplankton grazing in the coastal Gulf of Alaska: Variations in top-down control of phytoplankton. *Limnology & Oceanography*, *52*(4), 1480–1494. https://doi.org/10.4319/lo.2007.52.4.1480

Suryan, R. M., Arimitsu, M. L., Coletti, H. A., Hopcroft, R. R., Lindeberg, M. R., Barbeaux, S. J., et al. (2021). Ecosystem response persists after a prolonged marine heatwave. *Scientific Reports*, *11*(1), 6235. https://doi.org/10.1038/s41598-021-83818-5

Verity, P. G., & Lagdon, C. (1984). Relationships between lorica volume, carbon, nitrogen, and ATP content of tintinnids in Narragansett Bay. *Journal of Plankton Research*, *6*(5), 859–868. https://doi.org/10.1093/plankt/6.5.859

Waite, J. N., & Mueter, F. J. (2013). Spatial and temporal variability of chlorophyll-a concentrations in the coastal Gulf of Alaska, 1998–2011, using cloud-free reconstructions of SeaWiFS and MODIS-Aqua data. *Progress in Oceanography*, *116*, 179–192. https://doi.org/10.1016/j.pocean.2013.07.006

Weingartner, T. J., Danielson, S. L., & Royer, T. C. (2005). Freshwater variability and predictability in the Alaska Coastal Current. *Deep Sea Research Part II: Topical Studies in Oceanography*, *52*(1–2), 169–191. https://doi.org/10.1016/j.dsr2.2004.09.030

Wu, J., Aguilar-Islas, A., Rember, R., Weingartner, T., Danielson, S., & Whitledge, T. (2009). Size-fractionated iron distribution on the northern Gulf of Alaska. *Geophysical Research Letters*, *36*(11), L11606. https://doi.org/10.1029/2009GL038304